KTH Electrical Engineering

On Magnetic Amplifiers in Aircraft Applications

Lars Austrin

ELECTROMAGNETIC ENGINEERING
SCHOOL OF ELECTRICAL ENGINEERING

ROYAL INSTITUTE OF TECHNOLOGY
SWEDEN

Submitted to the School of Electrical Engineering, KTH,
in partial fulfillment of the requirements for the degree of
Licentiate of Technology.

Stockholm 2007

Lars Austrin
Saab AB,
Saab Aerosystems
SE-581 88 Linköping

Royal Institute of Technology
Electromagnetic Engineering
SE-100 44 Stockholm
Sweden

Cover Photo, JAS39A and JAS39B, by: Katsuhiko Tokunaga

Akademisk avhandling som med tillstånd av Kungl Tekniska Högskolan framläggs till offentlig granskning för avläggande av teknologie licentiatexamen 2007-06-08 kl 11.30 i sal H1, Teknikringen 33, Kungl Tekniska Högskolan Stockholm.

TRITA-EE-2007-20
ISSN: 1653-5146
ISBN 978-91-7178-664-7
© Lars Austrin, Stockholm, 2007

Abstract

In the process of designing an electric power supply system for an aircraft, parameters like low weight and low losses are important. Reliability, robustness and low cost are other important factors. In the Saab Gripen aircraft, the design of the primary power supply of the electric flight control system was updated by exchanging a switching transistor regulator to a magnetic amplifier (magamp). By introducing a magamp design, weight was saved and a more reliable power supply system at a lower cost was achieved.

In this particular case, with the power supply of the electric flight control system in the Saab Gripen fighter, advantage could be taken of a specific permanent magnet generator (PM-generator). The frequency of the generator offered the perfect conditions for a magamp controller. A key parameter in designing magnetic amplifiers (magamps) is low losses. New amorphous alloys offer new possibilities of the technique in designing magnetic amplifiers, because of their extremely low losses.

The core losses are evaluated by studying the equations and diagrams specifying the power losses. The core losses are evaluated and compared with the copper losses in the process of optimizing low weight and low losses. For this an engineering tool is developed and demonstrated.

Evaluations of the hysteresis characteristics for the magnetic alloys, as well as modeling and simulation of the core losses, are presented in this work. The modeling of the core losses includes hysteresis losses, eddy current losses and excess losses as well as copper losses. The losses are studied dynamically during realistic operational conditions. The model can be used for any generic analysis of hysteresis in magnetic circuits. Applications of magnetic amplifiers in aircrafts have been demonstrated to be a feasible alternative.

Keywords

- Magnetic Amplifier (Magamp)
- Amorphous
- Power Losses
- Control Winding
- Self-saturating
- Hysteresis
- Converter
- More Electric Aircraft (MEA)
- Inverter
- Power-by-Wire
- Dymola
- Permanent Magnet Generator (PM-generator)
- Transformer Rectifier Unit (TRU)
- Constant Speed Drive (CSD)
- Excess losses or anomalous losses
- Modeling
- Simulation
- Unmanned Aerial Vehicle (UAV)

Acknowledgements

This work has been supported by many persons from different organizations. First, I would like to express my thanks to my professor, Göran Engdahl, for his inspiration, guidance and experience shared with his students. I would also like to thank professor Roland Eriksson and my colleagues at KTH, Julius Krah, David Ribbenfjärd, Per Pettersson and Mohsen Torabzadeh-Tari for interesting discussions and important contributions as co authors.

To my colleagues at Saab, Eiwe Nilsson, and KG Fransson, I express my thanks for their support and interesting discussions.

The support by Saab management is represented by Lars Borggren, Peter Dickman and my tutor, PhD Birgitta Lantto, as well as the Saab research program directorate represented by Göran Bengtsson. Thank you for making this work possible.

Furthermore I would like to express my thanks to professor Petter Krus, PhD Björn Johansson, and Peter Hallberg for corporative works at LiTH.

Thanks to the sponsor, represented by Curt Eidefeldt, FMV, Erik Prisell, FMV as well as Owe Lyrsell, Lutab, whose support in the field of More Electric Aircraft technology has been essential for this work.

This work was financed by Saab Aerosystems and the Swedish National Aerospace Research Program (NFFP).

I must express my gratitude to my wife, Gun. Without her patience and support, this work would not have been possible. Finally I would express my appreciation to all colleagues, family, and friends who have supported and encouraged me during the process.

Stockholm and Linköping, June 2007 Lars Austrin

Contents

CHAPTER 1 INTRODUCTION 1

1.1 BACKGROUND 1
1.2 HISTORY 3
1.3 AIM 8
1.4 OUTLINE OF THE THESIS 10
1.5 LIST OF PUBLICATIONS 11

CHAPTER 2 THE MAGNETIC SWITCH 13

2.1 PRINCIPAL FUNCTION 13
2.2 MODE OF OPERATION 17

CHAPTER 3 THE MAGNETIC AMPLIFIER 19

3.1 TOPOLOGIES 19
  3.1.1 The Ramey Amplifier 19
  3.1.2 The Self Saturating Magamp 23
  3.1.3 The Three Phase Magnetic Amplifier 23
3.2 THE MAGAMP COMPONENTS 24
  3.2.1 Rectifier Diodes 24
  3.2.2 Cores 25
  3.2.3 Coils 25
  3.2.4 Control Winding 26
3.3 AVAILABLE ALLOYS 27
3.4 HEAT TREATMENT - ANNEALING 30
3.5 LOSS MECHANISMS 31
  3.5.1 The Static Hysteresis Losses 32
  3.5.2 Eddy Current Losses 33
  3.5.3 Excess Losses 33
  3.5.4 The Total Losses 33

CHAPTER 4 MAGNETIC AMPLIFIER DEMONSTRATORS 37

4.1 THE MAGNETIC AMPLIFIER DEMONSTRATOR 37
4.2 THE JAS39 GRIPEN MAGAMP 38

CHAPTER 5 MAGNETIC AMPLIFIER MODELS 43

5.1 EQUIVALENT CIRCUIT OF THE MAGNETIC SWITCH 43

5.2 THE CORE MODEL 45
  5.2.1 The Static Hysteresis Model 45
  5.2.2 Eddy current and excess loss phenomena 47
  5.2.3 The Equivalent Circuit of a Core Element 48
5.3 SIMULATION EXAMPLES 49
  5.3.1 Magamp Simulation 49
5.4 ANALYSIS OF LOSSES AND WEIGHT OF A MAGAMP CORE 60
  5.4.1 Graphical Analysis Example 61
5.5 A PROPOSED ENGINEERING TOOL 66
  5.5.1 Input Parameters 68
  5.5.2 Dimensioning-Calculation Examples 69
  5.5.3 Preliminary Interpretations of the Results from the Engineering Tool 73
5.6 CONCLUSIONS 74

CHAPTER 6 SYSTEM INTEGRATION IN AIRCRAFT APPLICATIONS 77

6.1 AIRCRAFT POWER SUPPLY SYSTEMS 77
6.2 FUTURE POWER SYSTEMS 79
  6.2.1 Skin Effect in Wiring 80
  6.2.2 Increased Impedance in Wiring 82
6.3 FEASIBLE CONCEPTS 84

CHAPTER 7 CONCLUSIONS AND FUTURE WORK 89

7.1 CONCLUSIONS 89
7.2 FUTURE WORK 90

REFERENCES 91

LIST OF SYMBOLS 95

APPENDIX 97

INDEX 98

Chapter 1

Introduction

1.1 Background

Historically, Magnetic Amplifiers (Magamps) have had an important role for regulation and control of electric power in different applications, especially prior to the use of semiconductors.

This technology is attractive in More Electric Aircraft (MEA) systems due to the possibility to achieve a compact, robust and a highly reliable design.

Nevertheless the technology is rather unknown, but deserves to be better known and to be used, due to the new possibilities offered. Producers of Switched Mode Power Supply, looking in to the possibility of using magamps in their products, experience that the learning curve to be able to use the technology is a concern [29]. As a part of this, it is important to inform about More Electric Aircraft (MEA) technology and magamps [4].

Magnetic amplifiers are used in the power supply of the Electronic Flight Control System in the Swedish "Gripen" fighter-aircraft. The first flight took place in 1988, and magnetic amplifiers were introduced in 1995. This aircraft is in service since 1997, and is expected to fly until 2040.

The Gripen magamp is designed to be a three-phase voltage regulator. Other applications are found in the Swedish fighter aircraft AJ37 Viggen, where a magamp is used for the excitation of the generator, i.e. for regulation of the main generator output-voltage. First flight, with this magamp in the generator system, took place in 1967. This aircraft was in service between 1971 and 2005.

In J 35 Draken, magamps were used for the navigation platform. First flight with this aircraft took place in 1955 and was in service 1959 and was flying until 2005.

Applications of new soft magnetic materials, such as amorphous magnetic alloys, have enabled usage of magnetic amplifier (magamp) technology in the design of competitive electric power regulators.

In the process of designing an electric power supply system for an aircraft, parameters like low weight and low losses are important [9]. Reliability, low maintenance and robustness are other important factors. In the Saab Gripen aircraft, the design of the primary power supply of the electric flight control system was updated by exchanging from a switching transistor regulator to a magnetic amplifier (magamp). By introducing a magamp design, weight was saved and a more reliable unit at a lower price was attained.

An electric power supply system for an aircraft is basically specified by Mil-Std-704, which specifies a 28 VDC system, a three-phase 115 VAC, a 400 Hz system, as well as a 270 VDC system. By comparing the weight and size of the generators and transformers, with units of comparable rating for the commercial systems 50/60 Hz, it can be noted that the aircraft units have a significantly lower weight due to the higher frequency. In the particular case with the power supply of the electric flight control system in the Saab Gripen fighter, advantage could be taken of a specific permanent magnet generator (PM-generator), supplying a variable voltage and a variable frequency between 2400 and 4000 Hz. The higher the frequency, the higher is the potential for weight savings. The weight is roughly proportional to the inverse of the frequency [5].

In the trend of More Electric Aircraft designs [9], with a power supply of 270 VDC, the used power-generators commonly work at a higher frequency than 400 Hz. One question is then whether advantage can be taken of a higher operating frequency.

A key parameter in designing magnetic amplifiers (magamps) is low losses. New amorphous alloys are opening up new possibilities of the technique of designing magnetic amplifiers by offering extremely low losses. The core losses can be evaluated by studying the hysteresis loop experimentally and/or by numerical simulations, or by studying equations or diagrams giving the power loss provided by manufacturers. Alternatively, the core losses can by verified in tests, where the losses are evaluated by electric or thermal methods.

1.2 History

Historically magnetic amplifiers were used in many different power supply applications. The magnetic amplifier is also called the saturable reactor or the transductor. A magnetic amplifier consists of electric and saturable magnetic circuits so interlinked that the reactance of an AC circuit is controlled by an independently applied magnetization.

The history of saturable reactors goes back to 1901 when C. F. Burges and B. Frankenfield described different types of control circuits for DC controlled saturable reactors [13].

A very important development phase started 1912-1918 when Ernst Alexanderson showed a method for modulating high frequency alternating currents from one of his alternators so that it could be used for transatlantic radio telephony [13].

A still preserved part of the history is the transatlantic telegraphic transmitter in Grimeton, south of Gothenburg in Sweden. See Fig. 1.

The radio transmitter was made a World Heritage in 2004. The telegraphic transmitter in Grimeton is using the Alexanderson system. The control circuitry is based on a magnetic amplifier. The heart of the power system is an alternating-current generator and a magnetic amplifier, which was developed by the Swedish engineer.

The designer Ernst Alexanderson was born in Sweden in 1878. With a degree from the Royal Technical Institute in Stockholm, he joined General Electric 1902.

Ernst Alexanderson was employed by Charles Steinmetz at General Electric in Schenectady. Steinmetz [18] is referred to in chapter 3.5.1, due to his work with iron losses. Alexanderson was the holder of 344 patents [15]. He was pioneer in radio, first employed at General Electric in Schenectady and later chief engineer at Radio Corporation of America (RCA).

Se Fig. 1. The World Heritage “Grimeton transatlantic telegraphic transmitter”

The radio transmitter consists of the following components, the generator, the transformer, the magnetic amplifier, and the capacitors. Other important components are the telegraphic key, and the relay. See Fig. 2, 3 and 4.

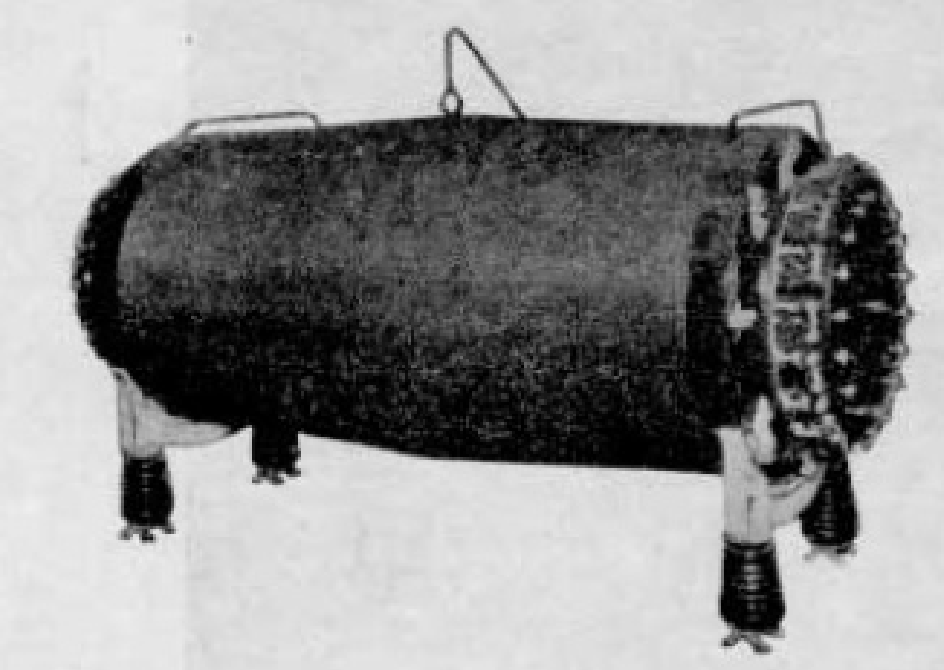

Fig. 2. The transformer, T, in the telegraphic transmitter

The transmitter used a frequency of 17200 Hz, generated by two generators rated at 200 kW. Only one generator remains today. The speed was 2115 rpm with 976 poles. The output from the alternators is routed through a transformer to the antenna. The output voltage from the transformer is 2000V [24].

In the transformer, a magnetisation-winding is shortening the antenna-transformer when no signal shall be transmitted.

The magnetization winding in the magnetic amplifier is controlled by a telegraphic key, feeding 250 Volt DC to saturate the Magnetic amplifier. The magnetic amplifier has the dimensions of approximately 1.0 x 0.7 x 0.5 m (h x w x d). See Fig. 3.

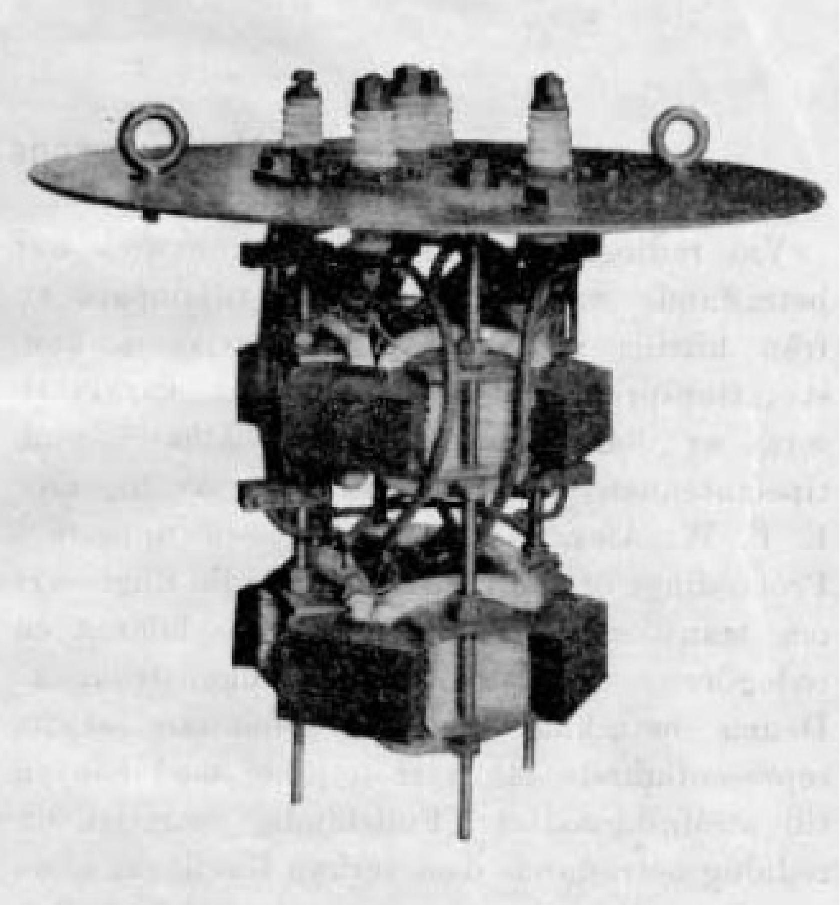

Fig. 3. The magnetic amplifier in the transmitter in Grimeton

The communication across the Atlantic did not function well during World War I and the need of telegram traffic with United States of America was demanding.

The Swedish Parliament therefore decided in 1920 that a Swedish long wave transmitting station and a receiving station should be built under the direction of the Swedish "Telegrafverket".

In the autumn of 1923, the establishment was ready, except for the six 127 meter antenna towers which were delayed one year because of strikes at the ironworks. The towers were placed at intervals of 380 meters with the 46 meter cross-arms on top carrying eight copper wires, which made up the antenna capacitance and the power supply to the six vertical radiating elements.

In December 1924, the radio station Grimeton went into traffic with the call signal SAQ.

In July 1925, the establishment was formally inaugurated by Swedish King Gustaf V and the designer Ernst Alexanderson [21].

Operational Function of the Alexanderson Magamp

The magnetic amplifier used in the telegraphic transmitter in Grimeton is based on a four-legged core see Fig. 4. The magnetic amplifier operates by switching the mode between saturated and unsaturated state of the magamp M controlled by the telegraphic key [24]. The basic circuit, a parallel connected saturable reactor, is topologically nearby the same as in the basic circuit in Fig. 8.

The signal source is an electric high speed generator, G, giving the frequency 17200 Hz. An ironless transformer, T in Fig 2 and 4, with 2 turns on the primary side is transforming the generator output power to 2000 V and 100 A. The magamp with the power winding, A, short-circuits the antenna by short-circuiting the transformer secondary winding, S in Fig 4, when no signal shall be transmitted.

The magamp, M in Fig. 4, is based on a four leg core with a power winding, A, and a control winding, B. The winding, A, consists of two anti parallel windings.

The magamp in the telegraphic sender operates in the following way:

- When not sending: the telegraphic key, K, is open, the relay, R, is closed, the control winding, B, is powered by the control voltage of 250VDC, the core in the magamp, M, is saturated. As a consequence of the saturated core, the power winding, A, is exposed as a very low copper wire resistance. The power winding, A, is then shortening the load i.e. by shortening the transformer. Less than 10% percent of the generator output can then reach the antenna. The magnetic switch in the magamp is closed.

The power winding, A, short circuits the antenna signal in series with the capacitor, C. The purpose of the capacitor, C, is together with the reactance of the winding, A, to minimize the short-circuit impedance by resonance for the used frequency.

- When sending: the telegraphic key, K, is closed, the relay, R, is open, the control winding, B, is open. The magamp is designed so that the two power windings, A, do not saturate the core, the magamp is open. The power winding, A, represents high impedance and is not conducting.

Due to the operational principle with the magamp short-circuiting the antenna, considerable heat is generated. Therefore the magamp requires oil cooling.

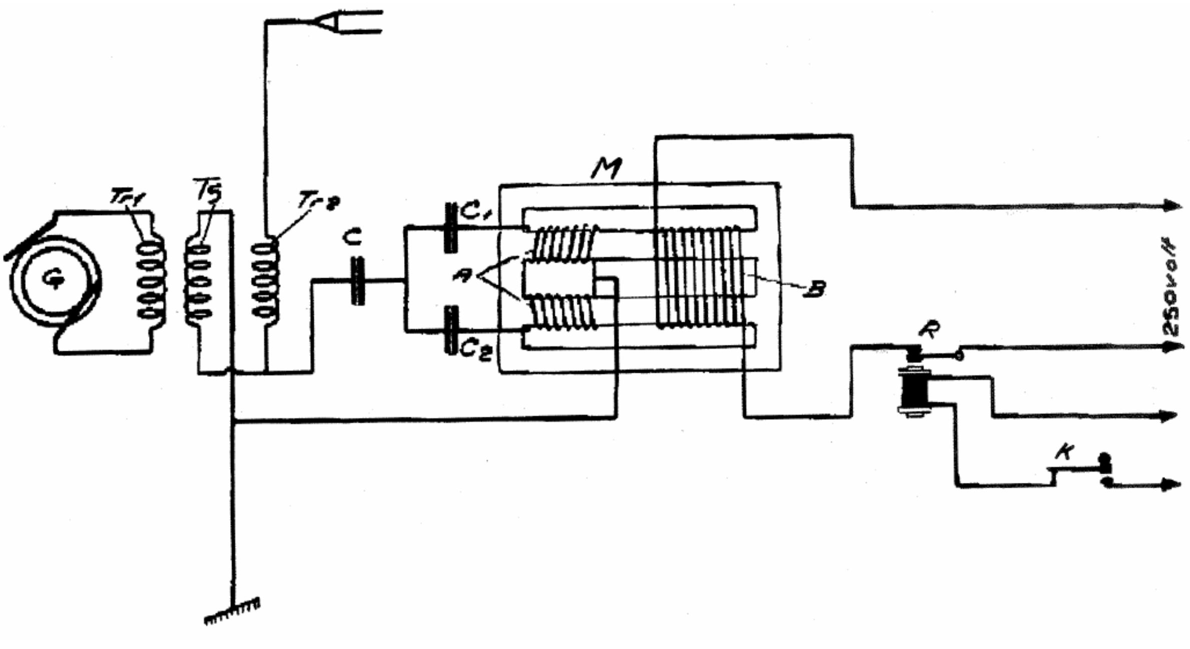

Fig. 4. Circuit diagram for Magnetic amplifier in Grimeton transmitter

The purpose of the capacitors, C_1, and, C_2, is to block the low frequency signal initiated from the telegraphic key, K.

One reason of the increased interest in magnetic amplifiers was the successful German technical development regarding various military applications, especially for naval fire-control systems, as such for the heavy cruiser "Prins Eugen" [13].

Important Swedish contributions were made by ASEA and inventers like U. Lamm, S.E. Hedström, and B. Nordfeldt [13].

Another interesting magamp application is a Stereo HiFi amplifier based on magnetic amplifiers offered to the market during a few years in the mid eighties by Lundahl Transformers [25]. The designer, Lars Lundahl, based the design on Ramey amplifiers, see Fig. 13. During a visit to Lundahl Transformers in 2004, the author had the opportunity to enjoy the excellent sound of his Stereo HiFi magnetic amplifier [49].

1.3 Aim

The trend in More Electric Aircraft technology is very much driven towards a simplification of the systems and to avoid complex mechanical systems. The other side of the coin might be huge and complex electronic power systems. The power electronic systems are expected to offer system simplification and advantages like a simplified installation. Nevertheless, new concerns arise due to the indicated required power levels of 1 MW of electric power in future commercial aircraft. These power levels stress the importance of reliable and rugged electric power systems.

One important question then is if the magamp technology can find new applications to meet these new requirements in future aircraft systems.

The following topics regarding the exploration of the potential of magnetic amplifiers are described in this thesis.

- Operation principles

The aim is, to review and analyze the basic circuitry [1] of the magnetic amplifier, based on a one-phase circuit extended to a three-phase circuit and to review different principles of operation.

- Simulation models

The aim is, is to study losses in a three-phase magamp including copper and core losses by simulating the hysteresis characteristics for amorphous magnetic alloys. The losses and the efficiency of the magamp are studied by modeling and simulation of the cores, operating in a three-phase circuit.

The presented model includes static hysteresis, classical eddy currents, and excess losses [6].

Thereby power losses can be evaluated, which enables an optimization of the design.

The use of the hysteresis models to estimate the static and hysteresis loss and excess losses [6, 7] of core material is demonstrated. The losses and the power-density [kW/kg] can thus also be evaluated.

- Evaluation tools

The aim is, to get an engineering tool for analyzing weight and volume [2]. Impact on weight and performance as a function of different magnetic material and operating frequency, are studied. The demonstrated modeling approach is considered to be one important dimensioning tool regarding future development of reliable devices for power management in MEA systems.

Power-density is of vital importance in an aircraft application. This implies the need for analyzing tools, stressing the limits of the current density, as well as optimising the chosen soft magnetic materials, regarding flux density B [T] and core losses.

- System integration

The aim is, to study a complete system with magnetic amplifier applications in an aircraft installation.

1.4 Outline of the Thesis

Chapter 1. The Introduction; gives a historical background as well as the motivation of this work on Magnetic Amplifiers.

Chapter 2. The Magnetic Switch; describes the fundamental parts of the magnetic amplifier, i.e. the cores and the copper windings. This gives a basic insight in the operational principles and design of a magnetic amplifier.

Chapter 3. The Magnetic Amplifier; describes how the magnetic switches in chapter 2 can be used in operating units. Normally a three phase magnetic amplifier is designed by three one-phase magamps connected to a six pulse rectifier bridge, giving a total of 12 rectifying diodes. The presented three phase magamp circuit, with 6 rectifying diodes, represents a simplification used in this work. Power circuits and available components, as well as some design considerations are also presented.

Chapter 4. Magnetic Amplifier Demonstrators; describes the author's work with the design of the magamp demonstrator and the final production unit for the JAS39 fighter, as produced by Euro Atlas in Bremen.

Chapter 5. Magnetic Amplifier Models; a three phase magamp model is implemented in the simulation program package Dymola. This model was used to study the losses in a magamp application is to be able to estimate the losses for different operating frequencies, and is able to manage the nonlinear magnetic properties during transition from non-saturated to a saturated state of the core. Important contributions to the setup of this model were done by D. Ribbenfjärd and G. Engdahl.

An engineering tool for conceptual design of magnetic amplifier is also described in this chapter. The developed tool is based on core loss data supplied by the producers. These data, graphically presented for different materials have been expressed as equations for use in the engineering tool. A number of test examples show that a magamp design can be optimized for low losses or low weight. By choosing the right core material for a given operating frequency at a certain power rating, a design with coinciding weight and loss minima also can be achieved. A loss model of the core material that includes static hysteresis, eddy current and excess eddy currents is presented.

Chapter 6. Systems Integration in Aircraft Application; this chapter describes the system integration in aircraft applications. Possible concepts for future power generation and distribution system are described and analyzed with regard to frequency.

Chapter 7. Conclusion and Future work. Concludes the results and summarizes ideas for future work.

1.5 List of Publications

The following articles serve as a base for this thesis work:

[1] L. Austrin, J.H. Krah and G. Engdahl: "A Modeling Approach of a Magnetic Amplifier". *Proc. of the International Conference of Magnetism*, Rome, Italy, 27th July-1st August, 2003.

[2] L. Austrin, and G. Engdahl: "Modeling of a Three-phase Magnetic Amplifier". *Proc. of the 24th Congress of the International Council of the Aeronatical Science*, Yokohama, Japan, 29th August-3rd September 2004.

[3] B Johansson, L Austrin, G Engdahl, P Krus: Tools and Methodology for Collaborative Systems Design Applied on More Electric Aircraft. *Proc. ICAS 2004, Yokohama*, Japan, 29th August-3rd September 2004.

[4] L. Austrin, J. Hansson: New Electric Components for Aircrafts. Flygteknik, Proc. Flygteknik, Oktober 18-19, 2004 Stockholm (In Swedish).

[5] P. Krus, B. Johansson, L. Austrin: "Concept Optimization of Aircraft Systems Using Scaling Models". *Proc. Recent Advances in Aerospace Actuation Systems and Components*, November 24-26, 2004 Toulouse, France.

[6] L. Austrin, D. Ribbenfjärd, G. Engdahl: “Simulation of a Magnetic Amplifier Circuit Including Hysteresis”. *Digest for Intermag*. Nagoya, Japan, April 2005.

[7] L. Austrin, D. Ribbenfjärd, G. Engdahl: “Simulation of a Magnetic Amplifier Circuit Including Hysteresis”. *IEEE transactions*, to be published.

[8] Peter Hallberg, Lars Austrin, Petter Krus: “Low Cost Demonstrator as a Mean for Rapid Product Realization with an Electric Motorcycle Application”. *Proceedings of IDETC/CIE 2005*.

Chapter 2

The Magnetic Switch

In the previous chapter the concept magnetic amplifier (magamp) is used consequently and describes the complete unit including the magnetic elements, all required components for regulation and control, as well as rectifiers. The magnetic elements are based on copper and magnetic cores. To better clarify the operational function of the magnetic elements we hereby introduce the concept “magnetic switch”.

The concept “magnetic switch” describes the operational function of how the magnetic element can work as a switch.

2.1 Principal Function

The operation of a magnetic switch in a magamp is based on switching between unsaturated and saturated state of a magnetic core, see Fig. 5. When the core is saturated and the magnetic switch is conducting, the switch is on. During the following half cycle the magnetic switch can be reset to an unsaturated state such that it is not conducting.

Normally a magnetic switch operates with alternating current in the power winding and direct current in the control winding.

The magnetic switch can be designed with one core, equipped with a power winding and a control winding, see Fig. 5. The problem with this design is that it will operate like a transformer. This implies that the load current transforms a significant current to the control winding and the control circuit [14].

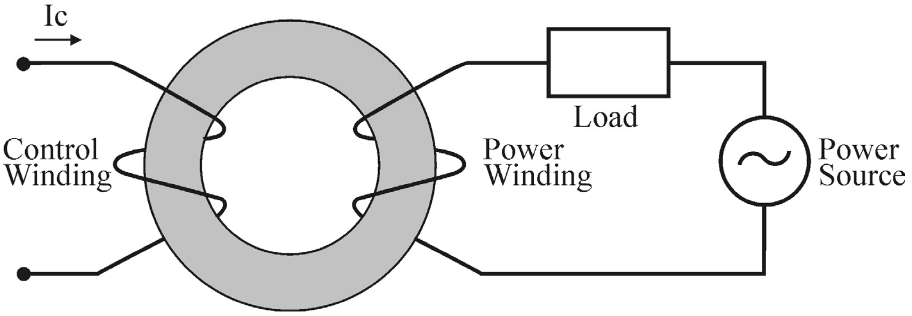

Fig. 5. The one-core magnetic switch

The basic concern is how to isolate the AC-power source from the DC-control circuit. This can be done with a resistor or an inductor in series with the control winding. A better solution is to use two cores balancing the imposed current from the power windings on the two serial connected cores. Principally this can be done by changing the control winding from clockwise to counter clockwise on the second core, see Fig. 6.

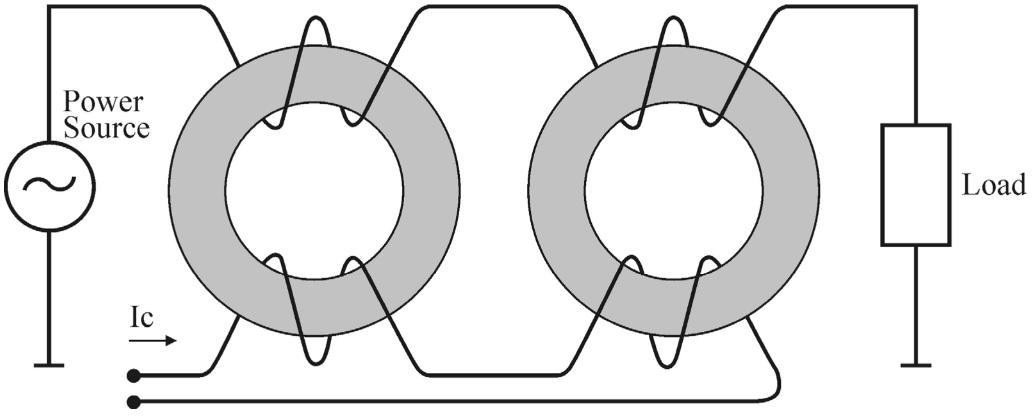

Fig. 6. The two core magnetic switch

The magnetic switch can be arranged in many different configurations. An alternative way is to use two cores with opposing power windings and one common control winding, see Fig. 7. The configuration in Fig. 7 and 8 shall be understood such that the cores shall be wound in such a way that the control winding will be a common winding for both cores, see Fig. 11. For the described circuits, the cores need an active control current for operating the magnetic switch. The unsaturated state implies a non conducting state, and a saturated state implies a conducting state.

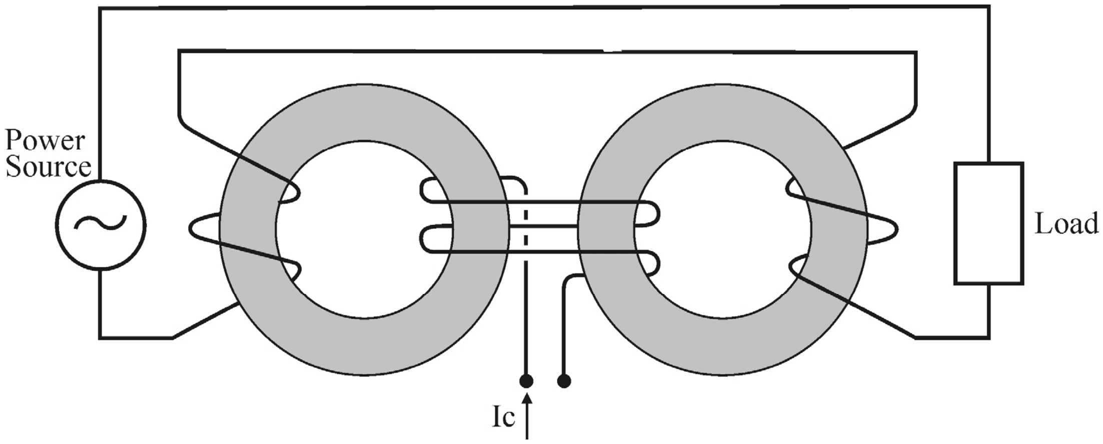

Fig. 7. Two cores with a common control winding

The shown circuits need an active control current. An active control current will saturate the cores and thus set the magnetic switch on. The control winding is used to change the operating point towards the levels of magnetic flux where saturation occurs.

An alternative configuration with opposing power windings is shown in Fig. 8.

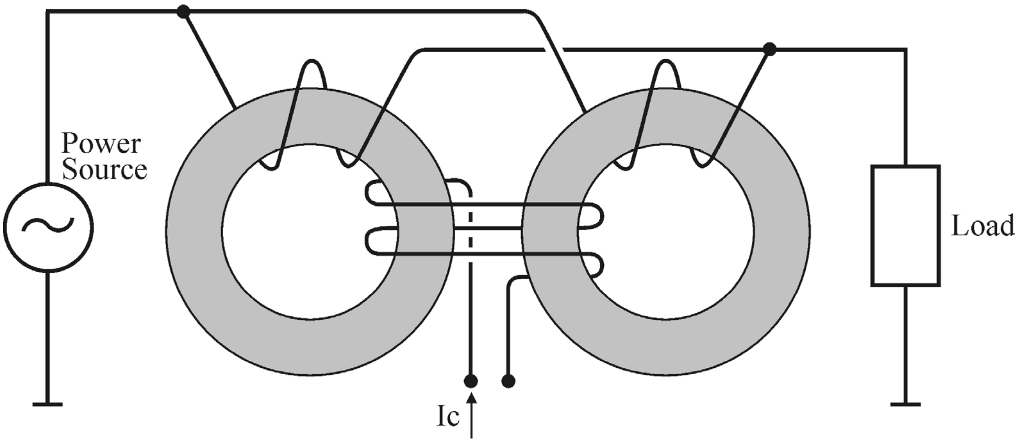

Fig. 8. Two cores with parallel power windings

The difference between the two core configuration in Fig. 6, 7 and 8 and the four legged core in Fig. 4 is mainly that the four core design is more costly. The described circuits operates in a similar way, however it can be noted that the matching of cores and windings are critical, not to achieve odd harmonic components of voltage induced in the control winding.

A typical encapsulated core is shown in Fig. 9. In this example the outer diameter is 37 mm and the weight is approximately 40 g.

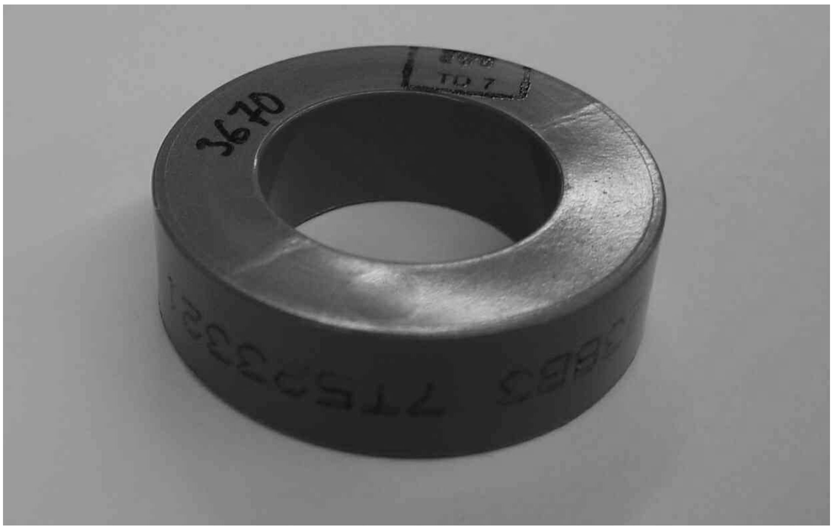

Fig. 9. A typical core for a magnetic switch (photo Euroatlas)

An example of a two core magnetic switch with separate control windings is shown in Fig. 10. In this example additional redundant windings are used.

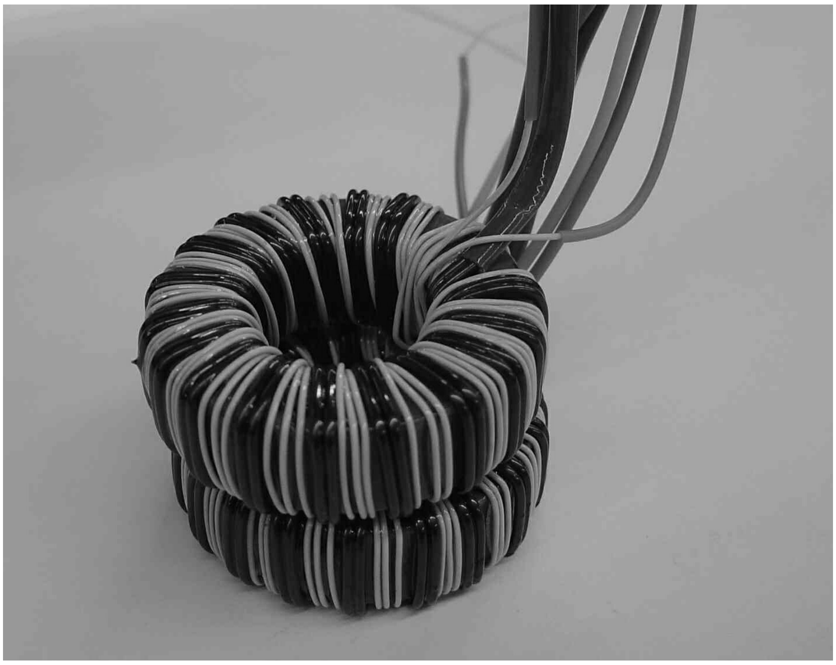

Fig. 10. A two core magnetic switch with separate control windings (Euroatlas)

In Fig. 11 an example of a magnetic switch with one common control winding can be seen. It can be noted that two power windings use a copper wire with a large area, while the control winding is very thin.

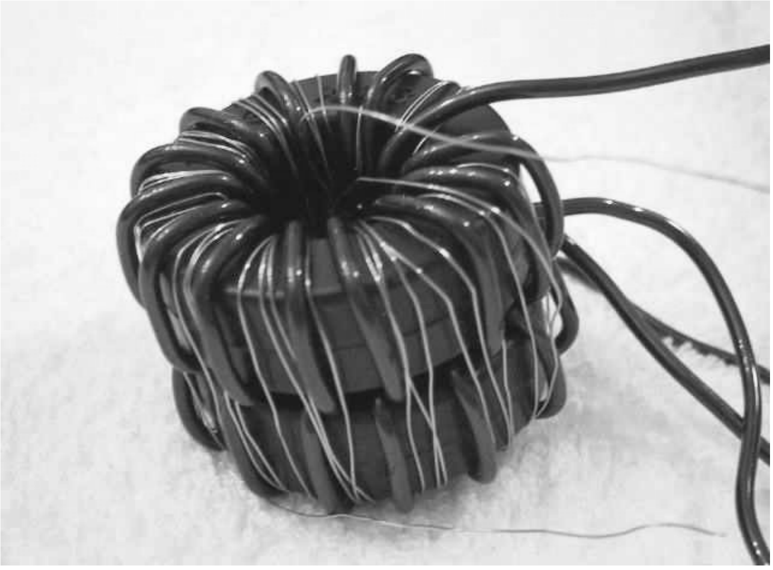

Fig. 11. Example of a two core magnetic switch with one control winding

2.2 Mode of operation

A magnetic switch can be used to regulate a considerable current in the power windings. This can be done with a control current of only a fraction of the output current. The control winding changes the mode of operation by moving the point of regulation, out from or in to the saturation area, see Fig.12.

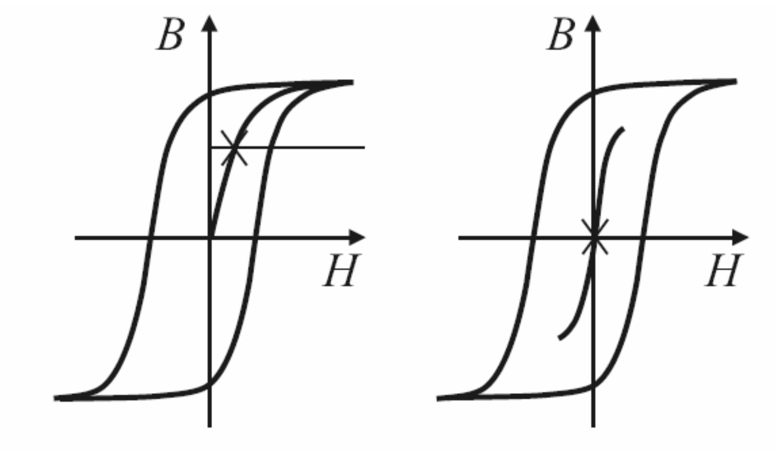

Fig. 12. Example of the magnetic characteristics

The circuits shown in Fig. 6-8 need active current in the control winding to saturate the cores and thus set the magnetic switches in conducting mode. See Fig.13.

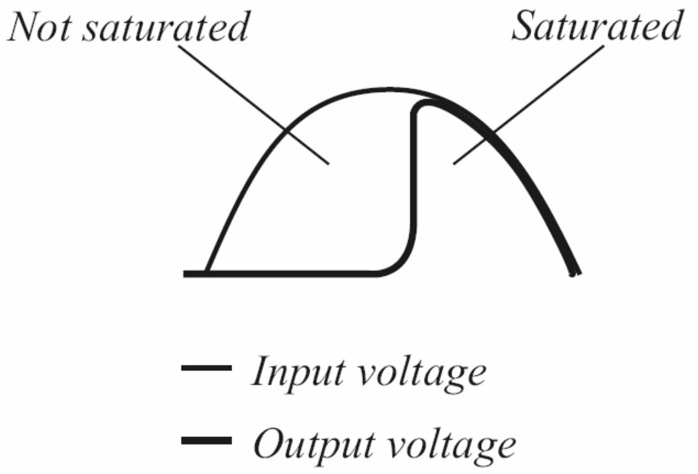

Fig. 13. Example of a wave form occurring in a magnetic switch during operation

Chapter 3

The Magnetic Amplifier

The expression magnetic amplifier (magamp) is used to describe the complete unit including the magnetic elements, all required components for regulation and control, as well as rectifiers.

3.1 Topologies

The magnetic amplifier comprises circuits shown in Fig. 6-8, with rectifying diodes such that rectified load-current saturates the cores. The magnetic switches will be set in a conducting mode until the saturation is removed by currents in the control windings.

The self-saturating magnetic amplifier will thus need control currents to take their cores out of saturation.

3.1.1 The Ramey Amplifier

The Ramey Amplifier, or with the alternative name, the “flux reset” magamp, is a voltage controlled magnetic amplifier.

The magamp is supplied by the AC power source, U_S, and is feeding the load, R_L. The magamp consists of a single wound core, M, in series with a rectifier diod and an inductor, L. The purpose of the inductor, L together with the capacitor, C, and the free wheeling diode, D, is to filter the output voltage.

The control of the output voltage is achieved by the voltage reference, U_{reg}. The circuit diagram of the Ramey amplifier [14] can be seen in Fig. 14.

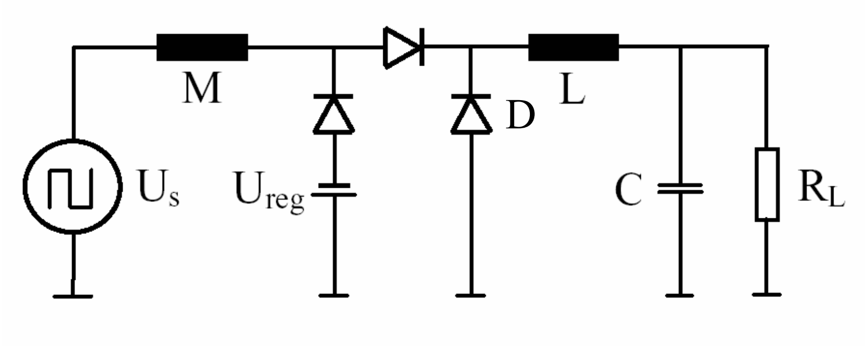

Fig. 14. The one-phase Ramey magamp

The rectifying diode handles the positive half period from the power source , U_S, which is filtered by the LC-filter and supplied to the load, R_L, as DC-power.

A typical application is voltage regulation in switched mode power supplies. The circuit however can be used for much more demanding requirements.

U_S is the signal from the power source where, T, is the period time. See Fig. 15a.

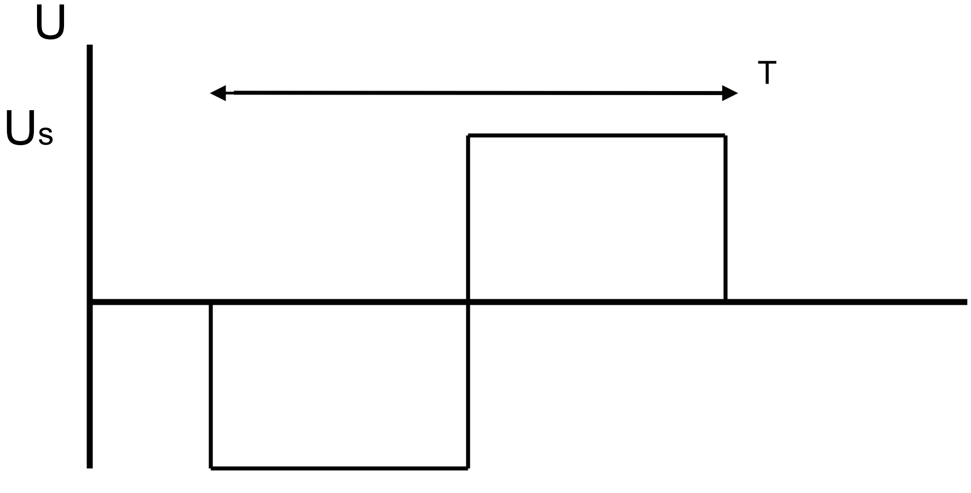

Fig. 15a. The generator signal U_S

In the Ramey amplifier the voltage time product for reset is given by U_S-U_{reg} and the duration, T/2, of the negative half period, represented by the area A.

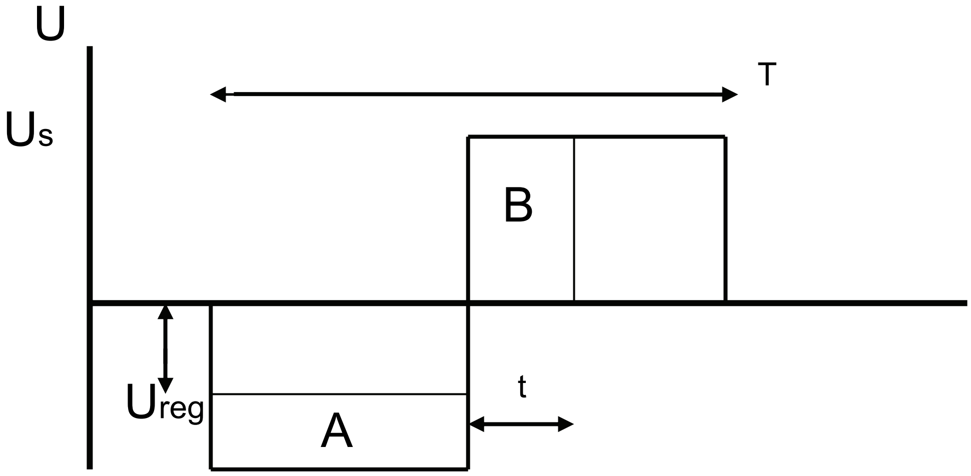

Fig. 15b. The operation characteristics for the Ramey magamp

The single wound core, M, is off and the magnetic core is unsaturated until the reset voltage time product is balanced and the switch is set on after the time, t. The voltage time area A, in Fig. 15b, produced by the control signal is during operation identical to the voltage time area B as described in Eq. (3.1).

The voltage time is "absorbed by the core" before the core saturates and the magamp is conducting the current, see Fig. 15c, which shows the magamp output. The rectifiers ensure that the two functions, reset area A and set voltage time area B are separated.

$$U_S \cdot t = (U_S - U_{reg}) \cdot 0.5 \cdot T \tag{3.1}$$

The response time of a magamp is normally 3-8 periods, depending if the magamp is self saturated or not, and is also depending on the inductance and resistance values in the circuit [11].

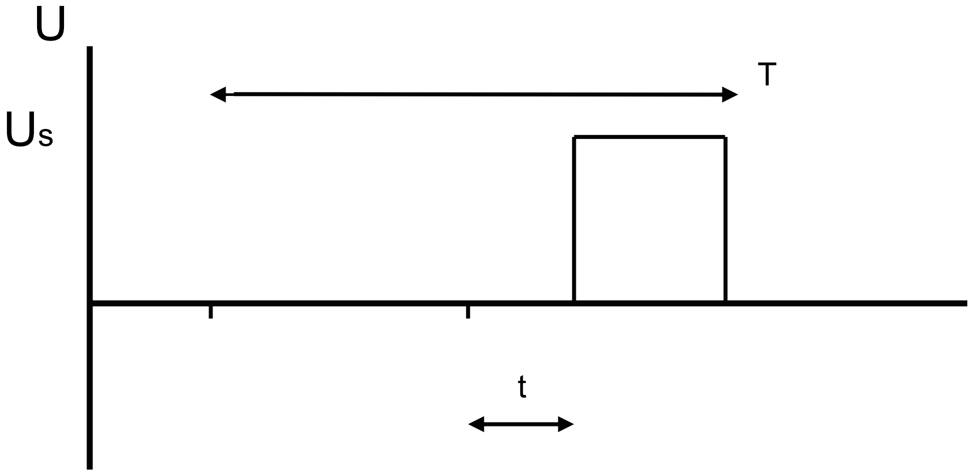

Fig. 15c. The output signal from the Ramey magamp

The advantage of this design is its simplicity and fast response.

A short response time, less than one period of the AC power source is achieved by permitting the voltage-time integral of the DC power source to reset the core to its operating point during the negative half period.

The Ramey amplifier can be supplied by a transistor switched mode power supply. The control by the voltage, U_{reg}, can be achieved by a transistorized control amplifier. The gain, phase and frequency response depend on the feedback from the control amplifier [30, 32] and the response of the control amplifier itself depends on its power supply [29, 31].

The ability for the magamp to handle the required voltage-time product $U \cdot t$ is depending on the number of turns, *N*, the core area, *A,* and the allowable flux, B, in the core. The equation for designing a Ramey amplifier can be expressed:

$$U \cdot t = 2 \cdot B \cdot A_{Fe} \cdot N \qquad (3.2)$$

The flux density span is $2B$, because the flux can be used over the whole span from negative to positive *B*.

3.1.2 The Self Saturating Magamp

With the self-saturating circuit in Fig. 16, a small control current I_C can be used to control the effective load voltage [1]. The functional elements are arranged such that a self-saturating circuit is achieved. In this design, a control current I_C is required for the cores to go from saturated to non-saturated state.

A magnetic amplifier is built up of a number of magnetic switches. Each switch comprises an arrangement with two amorphous ribbon wound toroidal cores as shown in Fig. 8. This configuration can easily by converted to a self saturating magamp by adding two rectifier diods, see Fig. 16. With the control current $I_c = 0$, the core will self-saturate and the switch is set on. By increasing I_c the state of saturation will be changed and the relative time of non-saturation will define the output voltage. In a magamp, all switch functions are realized by magnetic switches.

The one-phase magamp shown in Fig. 16 suffers from slow response time, due to the existence of circulating currents in the power windings.

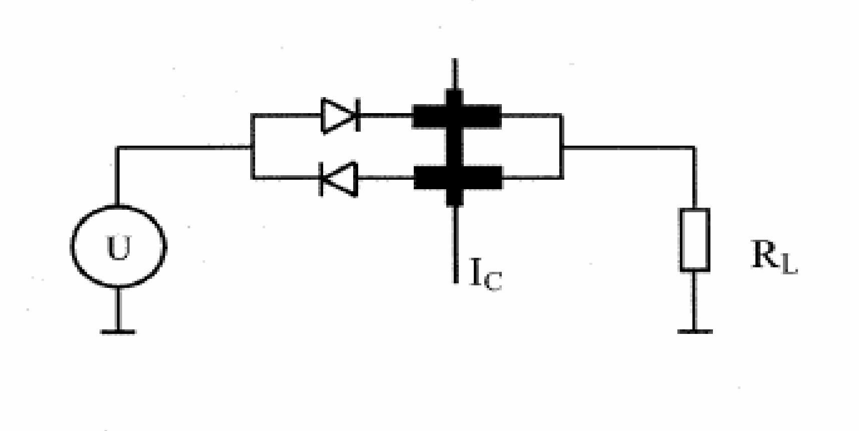

Fig. 16. The one-phase self saturating magamp

3.1.3 The Three Phase Magnetic Amplifier

The one-phase self-saturating circuit can be extended to a full 6-pulse design. See Fig. 17. The output from this magamp design comprises the combination of the three-phases yielding six rectified pulses through the load. The three-phase magnetic amplifier has a faster response time, compared to the one-phase magamp, since the circulating current will be limited by the load R_L.

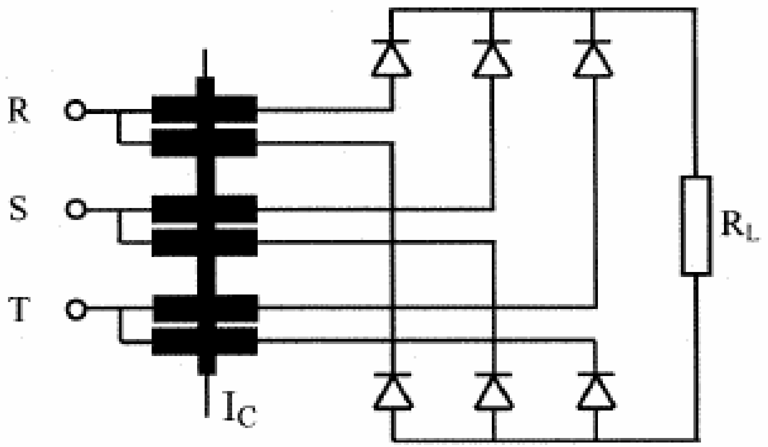

Fig. 17. The three-phase self saturating magamp

The magamp designed for the JAS39 Gripen is based on the block diagram in accordance with Fig. 17.

3.2 The Magamp Components

3.2.1 Rectifier Diodes

In the self-saturating magnetic amplifier rectifier diodes are needed. When designing a magamp, the voltage drop and corresponding power losses must be considered. The diodes must be mounted so the heat can be transferred away. A good rule is to use only half of rated voltage and current capability. Typical voltage drop of a silicone (Si) diode is about 1.5 volt. The junction temperature shall never exceed 150 [°C]. A design goal shall be a junction temperature below 100-125 [°C]. If higher temperatures are to be handled, semiconductors with SiC technology could be an opportunity. SiC rectifier diodes, now reaching the market, offer operation at higher junction temperature e.g. 250 [°C] but at a higher voltage drop, typically 3 volt. The rectifier diodes can be of bolt type or with a housing that can be attached to a cooling plate with a screw, as shown in Fig. 18.

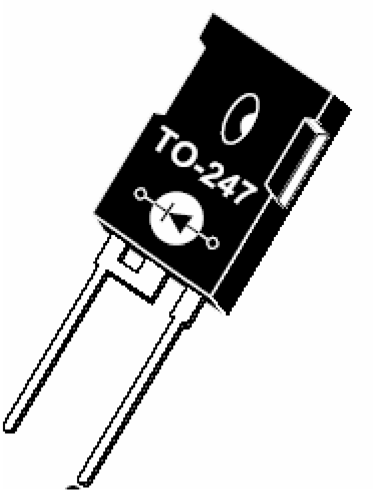

Fig. 18. A rectifier unit suitable for mounting on a cooling plate

3.2.2 Cores

The desirable material parameters have low coercivity force, and square-loop characteristics. In the process of choosing core material, high flux density may be contradictory to low losses.
An amorphous core is wound with many layers of the magnetic alloy, since the thickness of the core material is typically 0.022 mm.

The cores can have different shape, as an ordinary transformer or a toroidal core. The development of copper-winding machines enables the use of toroidal cores.

Annealed material (see paragraph 3.4) can easily loose its magnetic properties due to mechanical stress. Encapsulation of the cores in metallic or plastic cases reduces the risk of stressing them mechanically.

3.2.3 Coils

Normally the toroidal core is the base on which the copper is wound. Nevertheless, the opposite, with a prefabricated core, where the core is wound inside the copper-winding, has showed to be a successful concept as demonstrated by Lundahl Transformers, Norrtälje, Sweden [14].

3.2.4 Control Winding

The advantage of magnetic amplifiers is that large amplification can be achieved, and thus a thin control wire can be used. Other advantages can be the galvanic separation between the power source and the control winding, as well as the option with redundant control wiring.

The control of the magnetic amplifiers is easily attained by transistor circuits. In reference [33] a control circuit for a Ramey amplifier, which is minimizing the unwanted magamp reset signal is presented. This expands its controllable output signal.

A core with a large cross-sectional area and a short magnetic flux path length effectively yields a huge control gain [38] that can be in the order of 1:1000.

The deviation from perfect squareness of the core magnetization curve is defined by B_r/B_s, see Fig. 19. It must be considered during design but can according to the reference [28] be compensated for to some extent by the control circuitry. This is a topic for further analysis.

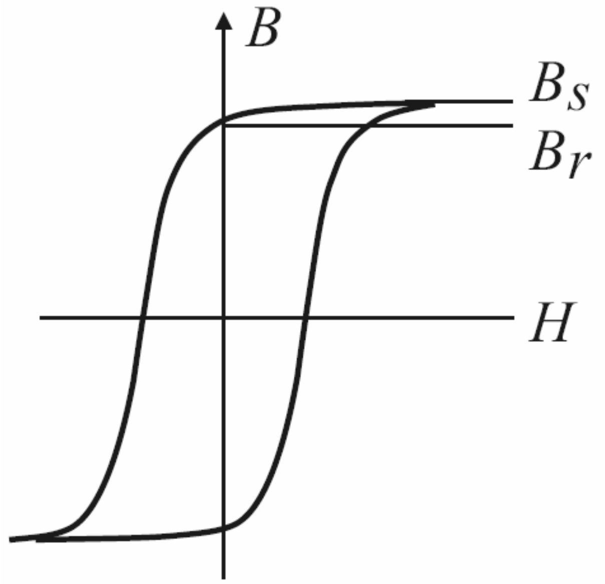

Fig. 19. The hysteresis characteristic

3.3 Available Alloys

The attractiveness of the magamp technology has increased during the last decades due to new soft magnetic materials that enable development of equipment with very high efficiency.

The core material for magamp applications shall have a rectangular magnetizing curve, with high relative permeability μ_r when non-saturated, high saturation flux B_s, and low coercitive force H_c [A/m]. In the saturated state, the permeability shall be low, i.e. the flux B shall change very little when changing the magnetic field. Most alloys are based or iron, nickel or cobalt.

Theoretically all soft magnetic materials can be used in a magnetic amplifier. However, just a few materials are suitable due to characteristics and losses. An important difference between different materials is the saturation level. Metglas 2605TCA has a saturation level of 1.56 [T] while Metglas 2714A has a saturation level of 0.57 [T]. The significant difference is that the use of the higher saturation materials enables a more compact design with lower weight. The Metglas 2605TCA will possibly offer slightly higher losses, but is offering a reduced weight of the core. Low weight is an important feature when utilizing the advantage of low losses.

Other materials as 4750 Alloy, Square Permalloy and Deltamax are alloys possible to use for magamp applications. The amorphous Metglas 2605TCA (similar to 2605 S-2), see Fig. 20, shows a very high squareness ratio B_r/B_s.

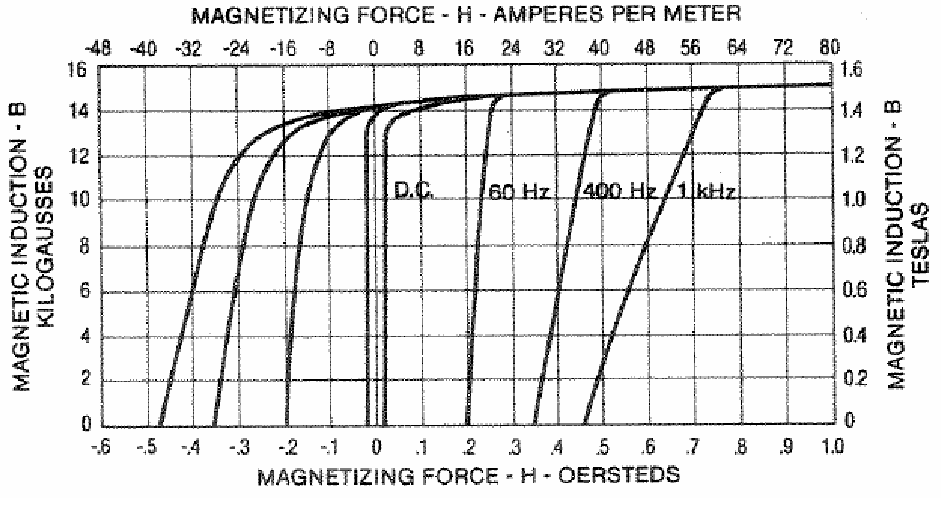

Fig. 20. Metglas 2605TCA characteristics

The amorphous alloys mentioned above show feasible characteristics for magamp applications.

The Deltamax is an alloy based on 50% nickel and 50% iron, and exhibits the highest squareness ratio B_r/B_s of the mentioned other materials. See Fig. 21. Deltamax has been available on the market for decades, today procured by Arnold. The material shows low losses and a very square hysteresis loop, despite this, the losses are approximately four times larger than for the amorphous Metglas 2605TCA.

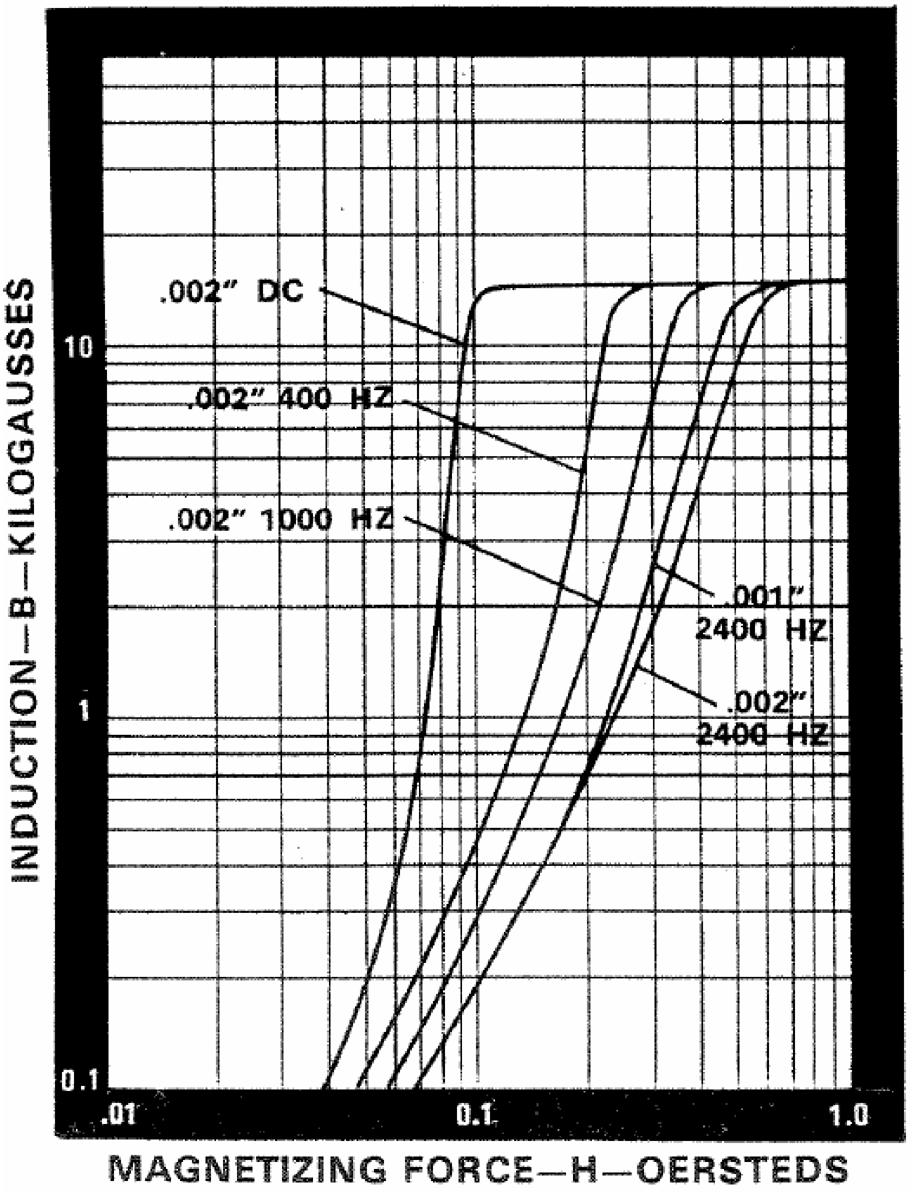

Fig. 21. Deltamax characteristics

The studied amorphous alloys are of interest in design of magnetic amplifiers due to their low losses at high frequencies and a high degree of squareness as defined by B_r/B_s,

The core losses of Metglas and Deltamax are given from the producer and are given per kilo or pound as a function of the flux, see Fig. 22 and 23.

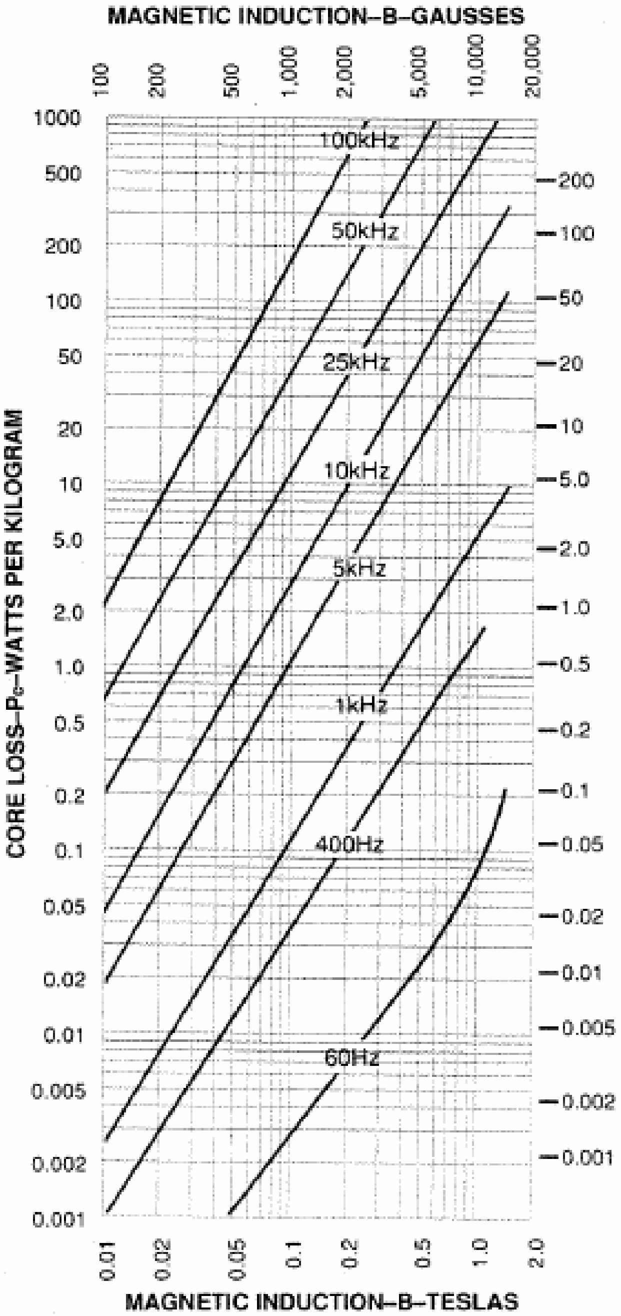

Fig. 22. Core losses for Metglas 2605 TCA

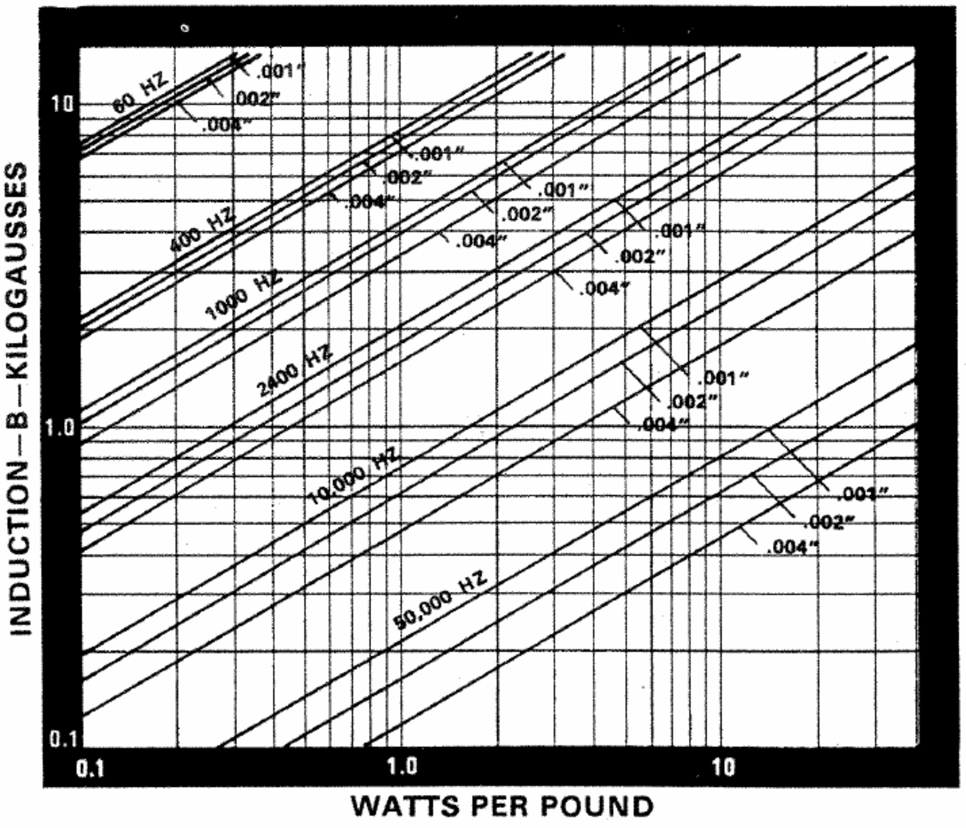

Fig. 23. Core losses for Deltamax

3.4 Heat Treatment - Annealing

Soft magnetic materials are often processed in different ways to achieve their optimal performance. Annealing of amorphous alloys is decreasing the coercivitive force H_C. The shape of the magnetization curve will then be closer to the desired rectangular hysteresis loop. The permeability in non-saturated state will also increase. The advantages achieved by annealing can by summarized as:

1. Lower losses due to the narrower hysteresis loop.
2. Faster switching with lower losses due to a rectangular hysteresis loop.
3. Increased permeability increases the control gain and thus reduces the control current.

The detailed annealing process might vary between different alloys and different suppliers. For information a comprehensive annealing process used by Saab is hereby summarized, see Table 1. Annealing is normally performed in an oven with an inert gas, where it is possible to magnetize the cores with a DC-current.

Table 1. Annealing data used by Saab

Time for annealing	1h
Temperature	350-400 [°C]
Magnetic field.	800 [A/m]

3.5 Loss Mechanisms

The magamp losses consist of:

- Core losses
- Copper losses in the power winding
- Diode losses
- Control losses from control circuits and copper losses in the control winding

In this thesis, the work is concentrated on the core and copper losses in the power winding.

The core losses can be divided into three different types:

- static hysteresis losses
- eddy current losses
- excess losses

3.5.1 The Static Hysteresis Losses

The static part of the magnetic hysteresis is by definition rate independent. This means that it is independent of frequency.

The static hysteresis losses can be explained as the frictional losses that occurs when the magnetic domains in the material move in respect to each other. The hysterisis losses can be evaluated by studying the core characteristics.

The area of the BH-loop represents the energy loss during one cycle and can be calculated according to:

$$W = \oint H dB \tag{3.3}$$

The power loss density [W/kg] can be expressed as:

$$P = \frac{f}{\rho} \int H \frac{dB}{dt} dt \tag{3.4}$$

where f is frequency [Hz]

ρ is weight per unit volume [kg/m^3]

H magnetic field [A/m]

B is flux density [T]

Note that the static energy loss per cycle is constant and frequency independent, but the power loss will be in proportion to the frequency.

The total core loss can be approximated as a function of frequency and the flux density and be expressed according to Eq. (3.5).

$$P = k_h \cdot f \cdot B_{\max}^n \tag{3.5}$$

k_h is a constant depending on the material and n varies between 1.5 and 2.5, according to Charles Steinmetz of General Electric company [18].

3.5.2 Eddy Current Losses

An AC magnetic field will always induce eddy current losses in conducting materials.

The classical eddy current losses in the core can be expressed as a function of B, f and the laminate thickness d of the magnetic material according to Eq. (3.6).

$$P_{eddy} = (2\pi f)^2 \hat{B}^2 \frac{d^2}{24\rho} \tag{3.6}$$

Where $\hat{B}$ is the amplitude of the geometrical mean flux density in [T], ρ is weight per unit volume in [kg/m^3] and d is the ribbon thickness in [m]

3.5.3 Excess Losses

Excess losses are depending on frequency up to the power of n. An increased frequency implies higher losses. The excess losses increase considerably with the operating frequency:

$$P_{exc} \sim f^n \tag{3.7}$$

n is a factor in the order of 1.5

3.5.4 The Total Losses

At lower frequencies the total core losses are the sum of hysteresis and eddy current losses.

$P_{hyst} \sim f$

$P_{eddy} \sim f^{2}$

$P_{exc} \sim f^{n}$

The complete core model includes static hysteresis losses, eddy current losses and excess losses. Examples of empirical expressions comprising all these losses is given in Eq. (3.9 and 3.10), [22].

$$P(t) = P_{hyst} + P_{eddy} + P_{exc} \tag{3.8}$$

The given power loss components are frequency dependent. The energy model can be shown per frequency which is equal to energy per cycle.

$W_{hyst} \sim =constant$

$W_{eddy} \sim f^{1}$

$W_{exc} \sim f^{n-1}$

The total energy losses W_{hyst} , W_{eddy} and W_{exc} of the magnetic material are shown graphically in Fig. 24.

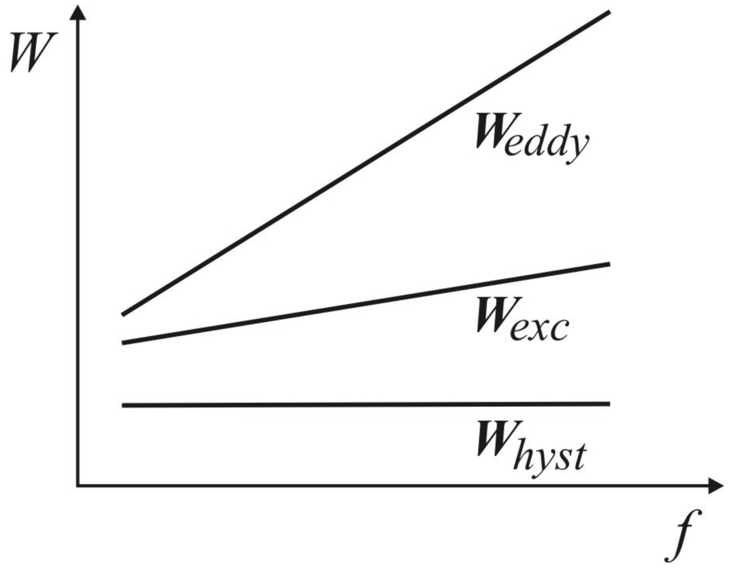

Fig. 24. The energy per cycle separated in different losses

The previous given expression for the total losses can be compared with the empirical equations for the total iron losses given by Metglas for the alloy 2714A [19]:

$$P = 9.93 \cdot 10^{-6} \cdot f^{1.57} \cdot B^{1.7} \qquad (3.9)$$

For the material 2605TCA core losses is graphically given in Fig. 22 by the manufacturer. The Eq. (3.10) is extracted from these graphs.

$$P = 88 \cdot 10^{-6} \cdot f^{1.57} \cdot B^{1.7} \qquad (3.10)$$

,which gives good compliance with the given data in Fig. 22 up to 10 000 Hz. These losses also are showed to be approximately 9 times bigger than those given by Eq. (3.9).

Chapter 4

Magnetic Amplifier Demonstrators

4.1 The Magnetic Amplifier Demonstrator

The magamp designed for the JAS39 Gripen is based on the block diagram in accordance with Fig. 17. In this chapter the demonstrator as well as the series unit is shown. This demonstrator was designed to verify the viability of the concept [8]. The design was done in a CAD system, but the unit was built by hand. The demonstrator fulfilled the purpose of demonstrating the concept, and served as a reference during the following design phase. In Fig. 25, a low cost demonstrator is shown.

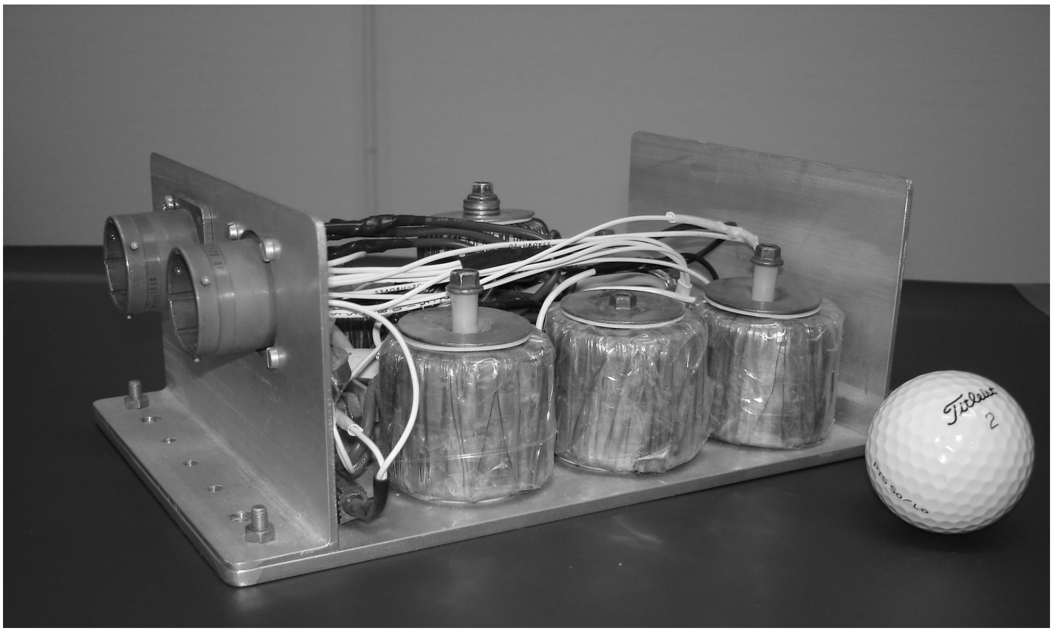

Fig. 25. The low cost magamp demonstrator.

4.2 The JAS39 Gripen Magamp

In Fig. 26, the wound components in the production unit can be seen for the three-phase magamp. The wound components in the rear end of the assembly are the magnetic switches. In the front end there are three transformers that are used for adapting the voltage level.

The size and weight of the magnetic switches are comparable to corresponding transformers of the same power rating with the difference that a secondary winding is not needed. In this particular case the smaller size of the adaptation-transformers can be explained by the fact that these are designed as autotransformers, which explains that size and weight is about half of the magnetic switches.

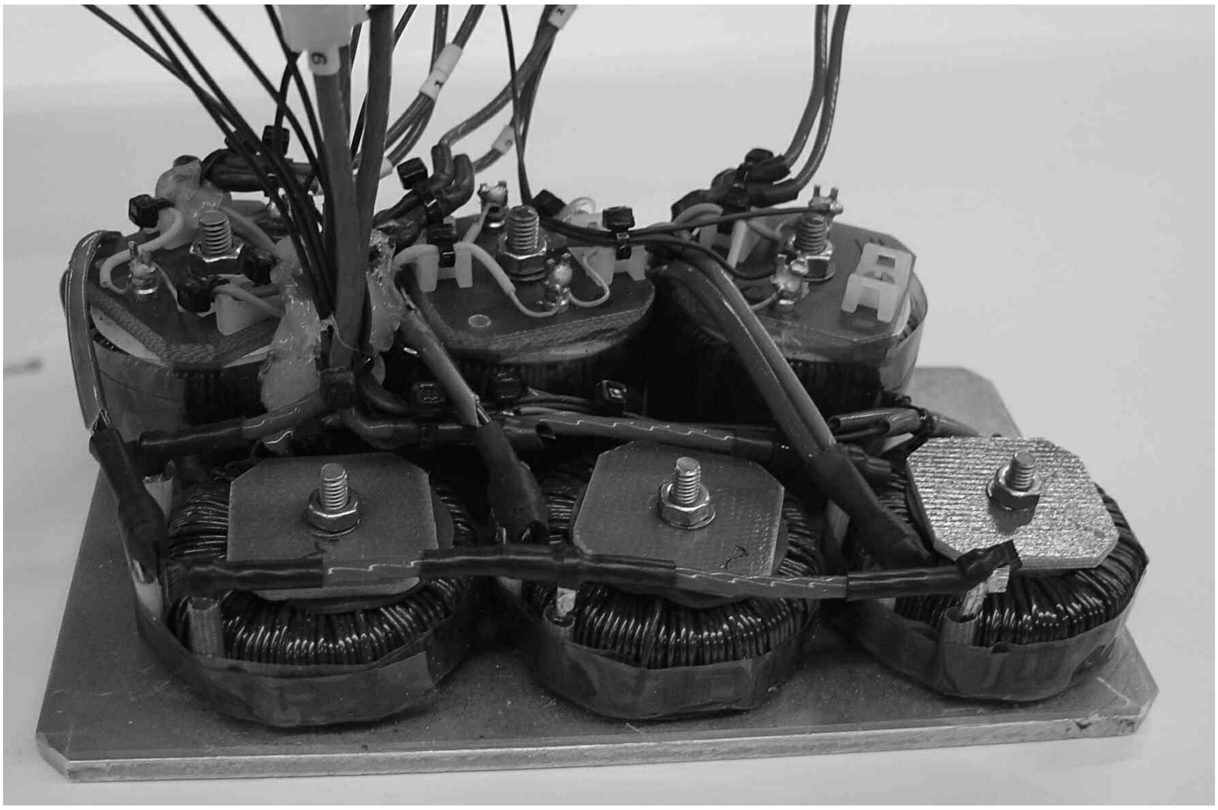

Fig. 26. The wound components in the three-phase magamp (photo Euroatlas)

In Fig. 27, the layout for the production unit can be seen. The main components are the magnetic switches, the transformers and the rectifier diodes which easily can be seen, see Table 2. The wound units in the final assembly are coated with gray/black 3M-coating. The coating is used to stabilize the windings to reduce risk of broken wires due to vibrations.

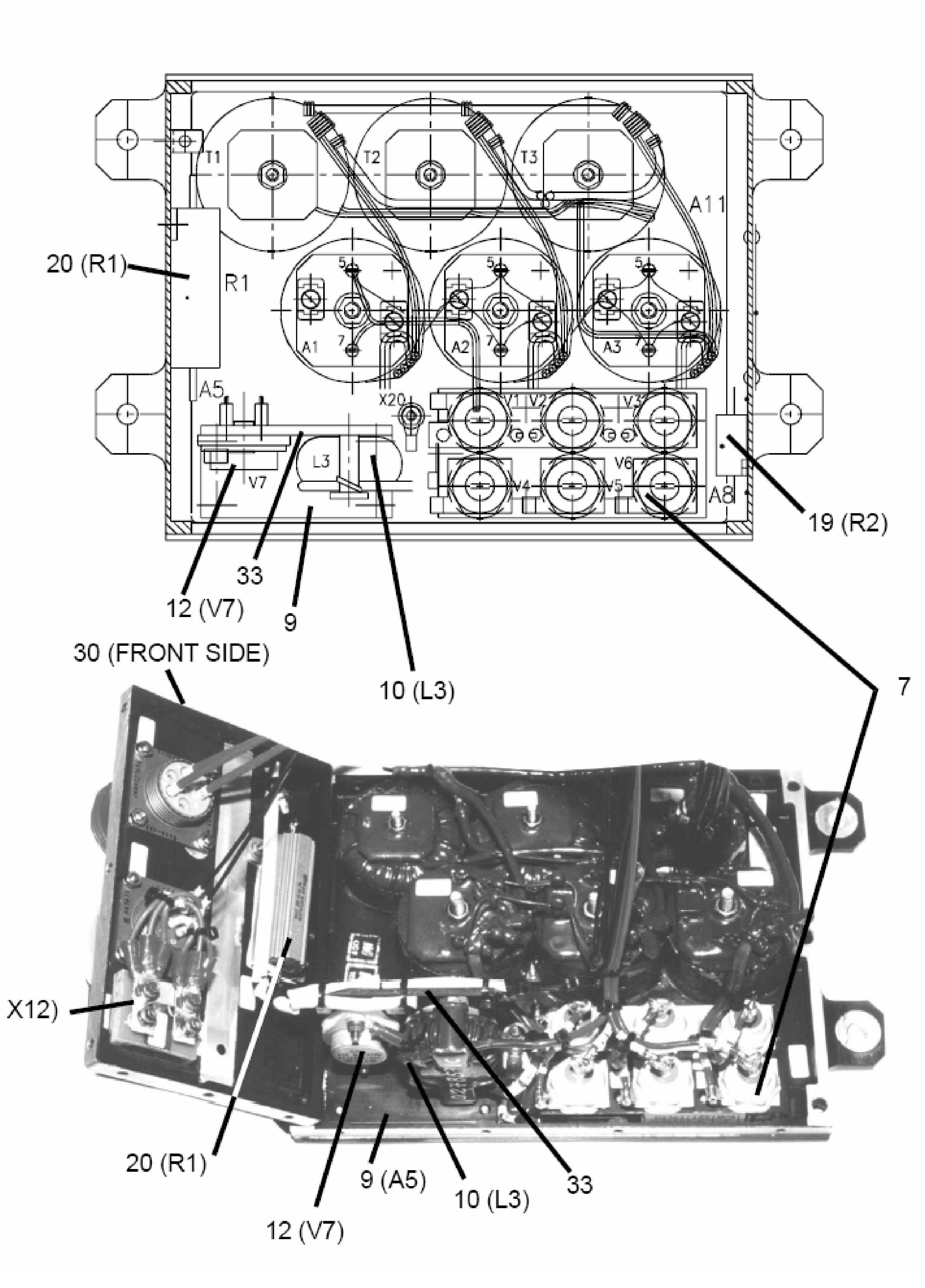

Fig. 27. The layout for three-phase magamp (photo Euroatlas)

Table 2. The vital components used in the CRU

A1-A3	magnetic switch
T1 –T3	transformers
7 (V1-V6)	rectifying diodes
10 (L3)	inductor (filter)
12 (V7)	overvoltage protection
20 (R1)	resistor

Fig. 28, shows the final assembly of the magnetic amplifier designed to supply the electronic flight control system in JAS 39 Gripen with a regulated voltage at 37 VDC. Weight of the complete unit, see Fig. 29, is approximately 3 kg.

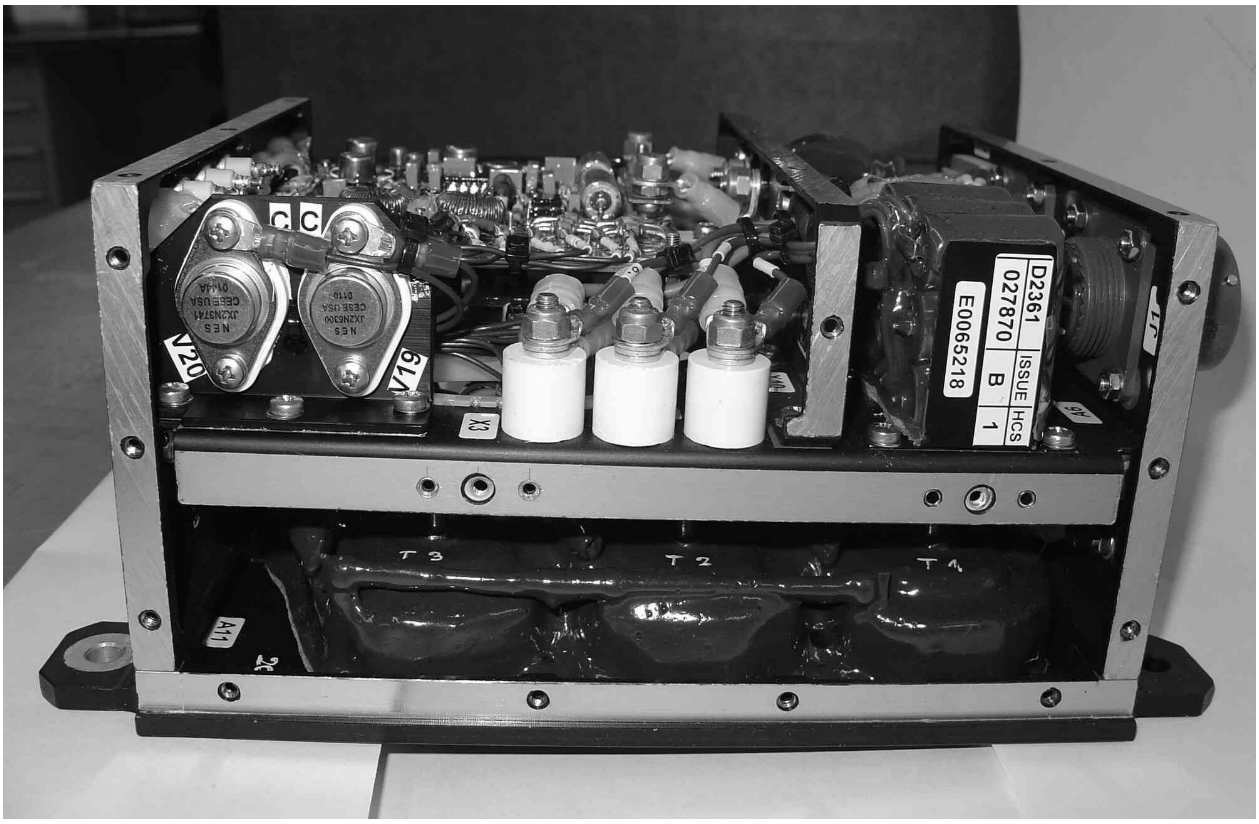

Fig. 28. The final assembly of the magnetic amplifier (photo Euroatlas)

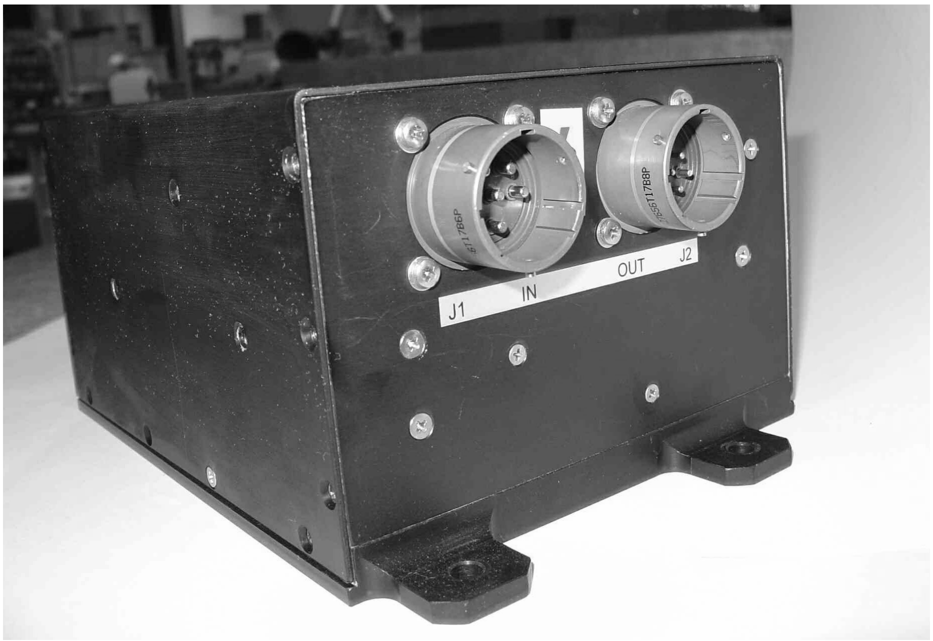

Fig. 29. The magnetic amplifier completed (photo Euroatlas)

The experience from the test and verification period indicates efficiency in accordance with expectations. The experience from the use in flight operations is that no failures of any kind have been reported.

Chapter 5

Magnetic Amplifier Models

5.1 Equivalent Circuit of the Magnetic Switch

In the process of analyzing a magnetic core during operation models for the magnetic properties such as model for hysteresis can be used. Simplified relations [5] constitute useful tools in the concept phase of a design that later is complemented with more detailed simulation models.

A circuit model is shown in Fig. 31. This model can be used to simulate the behaviour of a magnetic switch in a magamp circuit including static effects and stationary losses.

The basic functional arrangement of a magnetic amplifier comprises a magnetic core, usually in form of a two toroids with two load and one control winding, see Fig. 30.

Without current I_C in the control winding, the inductance of the load windings, is high, implying a switched-off condition. When I_C magnetically saturates the core, the load winding inductance will be low, implying a switched-on load condition.

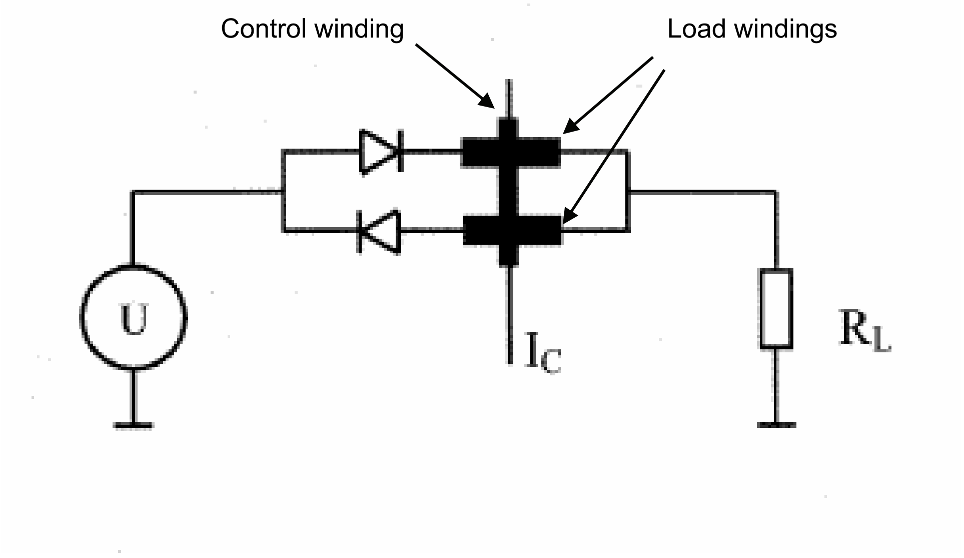

Fig. 30. Principal circuit of a one-phase magamp

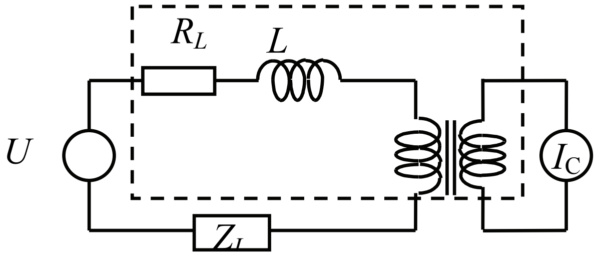

Fig. 31. Equivalent circuit of one phase of a simple magnetic amplifier

Equations (5.1) and (5.2) describing the circuit in Fig. 31 reveals that L needs not to be calculated explicitly [34]. N_L is the number of turns of the load winding. N_C is the number of turns of the control winding.

$$U - N_L A \frac{\partial B(H)}{\partial t} = (R + Z_L) \cdot I_L + L_\sigma \frac{\partial I_L}{\partial t} \qquad (5.1)$$

Fel! Objekt kan inte skapas genom redigering av fältkoder.
(5.2)

5.2 The Core Model

5.2.1 The Static Hysteresis Model

The Bergqvist model is based on that a magnetic material consists of a finite number n_p of pseudo particles, i.e. volume fractions with different magnetization

With no hysteresis present the magnetization would follow an anhysteretic curve, M_{an}. The hysteresis is introduced by using play operators for each volume fraction with plays equal to their pinning strengths.

In Fig. 32 the hystereses of a single pseudo particle with pinning force k and the anhysteretic curve, $m=M_{an}(P_k[H])$, where $P_k[H]$ is the play operator with play k, is illustrated.

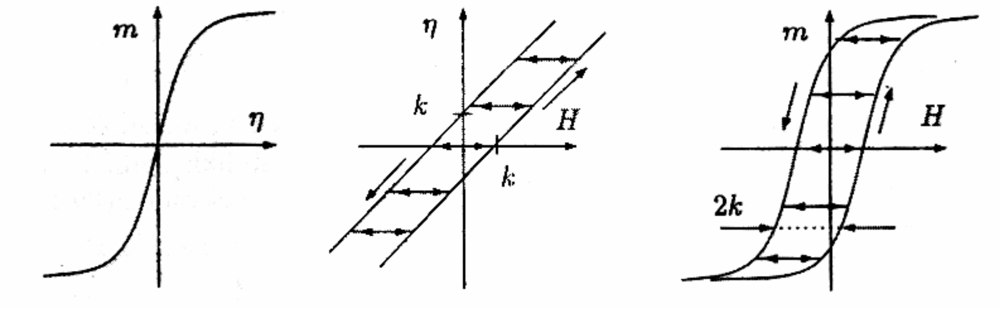

Fig. 32. The anhysteretic curve is shown to the left. In the middle the play operator function is illustrated. To the right the play function is combined with the anhysteretic curve giving the hysteresis model of a single pseudo particle.

By using a finite number of pseudo particles λ_i minor loops can be modelled. This is achieved by assigning individual pinning strengths $\lambda_i k$ to every pseudo particle i. Thus, the total magnetisation is given by a weighted superposition of the contribution from all pseudo particles, see Fig. 33.

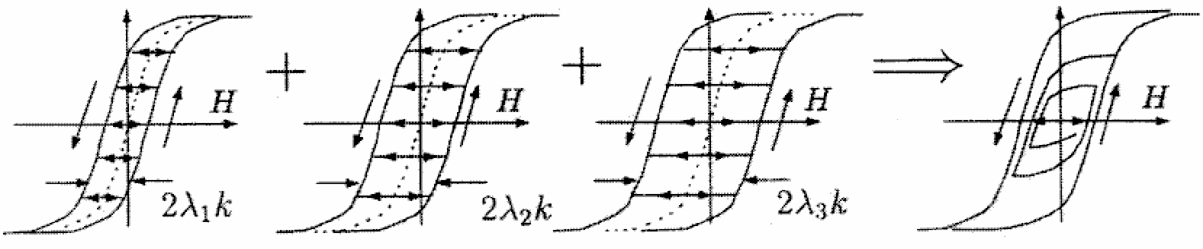

Fig. 33. Weighted superposition of the contribution from minor loops

The model of the hysteresis effect in the core is based on A. Bergqvist's magnetic hysteresis model [16]:

Fel! Objekt kan inte skapas genom redigering av fältkoder.
(5.3)

$$M[H] = c \cdot M_{an}(H) + \sum_{i=1}^{m} M_{an}(\mathrm{P}_{\lambda_i k}[H])\varsigma(\lambda_i) \tag{5.4}$$

where $\mathrm{P}_{\lambda_i k}$ i=1, 2…m are the play operators of the involved pseudoparticles λ_i with pinning strengths $\lambda_i k$ and volume densities $\varsigma(\lambda_i)$. M_{an} is the anhysteretic magnetisation curve, k the mean pinning strength and c magnetic reversibility constant. The magnetization model parameters are obtained experimentally by magnetic characterization of the core material. The following normalization conditions of $\varsigma(\lambda_i)$ are also valid.

$$c + \sum_{i=1}^{m} \varsigma(\lambda_i) = 1 \tag{5.5}$$

$$\sum_{i=1}^{m} \lambda_i \varsigma(\lambda_i) = 1 \tag{5.6}$$

The model stated above is rate independent i.e. it does not depend on the operation frequency. Therefore it is said to be static.

5.2.2 Eddy current and excess loss phenomena

The complete core model includes static hysteresis losses, eddy current losses and excess losses. An overall expression comprising all these losses is given in Eq (5.7) and (5.8) [22].

$$P(t) = P_{hyst} + P_{eddy} + P_{exc} \tag{5.7}$$

$$P(t) = P_{hyst}(t) + \frac{\sigma d^2}{12}\left(\frac{dB}{dt}\right)^2 + \frac{n_0 V_0}{2}\left(\sqrt{1+\frac{4\sigma G d w}{n_0{}^2 V_0}\left|\frac{dB}{dt}\right|}-1\right)\left(\frac{dB}{dt}\right) \tag{5.8}$$

The second term can be derived from Faraday's induction and represents the induced eddy currents. The last is suggested be G. Bertotti [22] and represents the excess losses.

The losses expressed in Eq. (5.8) correspond to the MMF drops according to Eqs. (5.9) and (5.10).

$$H_{eddy} = \frac{\sigma d^2}{12}\left(\frac{dB}{dt}\right) \tag{5.9}$$

$$H_{exc} = \frac{n_0 V_0}{2}\left(\sqrt{1+\frac{4\sigma G d w}{n_0{}^2 V_0}\left|\frac{dB}{dt}\right|}-1\right) sign\left(\frac{dB}{dt}\right) \tag{5.10}$$

5.2.3 The Equivalent Circuit of a Core Element

The governing idea is to model the core as series connected reluctance elements corresponding to static hysteresis, classical eddy currents and excess losses, see Fig. 34.

The MMF drop across the static hysteresis reluctance, the classical and the excess loss components described as counter MMF's are expressed in Eq. (5.11). where *h* is the length of the magnetic path.

$$\Theta(t) = N * I = R\Phi + \Theta_{eddy} + \Theta_{exc} = R\Phi + H_{eddy} * h + H_{exc} * h \qquad (5.11)$$

or with Eqs. (5.9) and (5.10) inserted.

$$\Theta(t) = R\Phi + \Theta_{cl} + \Theta_{ex} = R\Phi + \frac{h\sigma d^2}{12A}\left(\frac{d\Phi}{dt}\right) + \frac{hn_0V_0}{2}\left(\sqrt{1 + \frac{4\sigma Gdw}{n_0^{\,2}V_0A}\left|\frac{d\Phi}{dt}\right|} - 1\right) sign\left(\frac{d\Phi}{dt}\right)$$

Eq. (5.12)

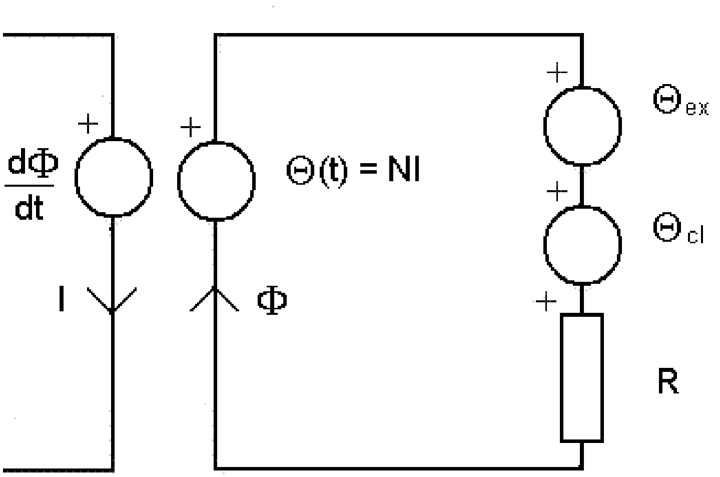

Fig. 34. A winding component circuit model of a single wound core with N turns

The first term of (5.10) originates from the static hysteresis model of A. Bergqvist [16]. The second term of originates from the classical eddy current model and the last term representing the excess losses from G. Bertotti [22].

$\Theta(t)$ represents the total resulting MMF drop in the core.

The parameters h and A are the bulk length and cross sectional area of the core respectively, σ the electrical conductivity of the core material and d the ribbon thickness. G is a parameter depending on the structure of the magnetic domains, n_o is a phenomenological parameter related to the number of active correlation regions when $f \rightarrow 0$, whereas V_0 determines how much micro structural features affect the number of correlated regions, w is the width of the ribbon [16].

The parameters n_o and V_0 can be determined indirectly by measurements of the core losses at different frequencies. The pure reluctance element represents the static hysteresis and is managed by the earlier presented hysteresis model [16]. The second term represents the occurring eddy currents in the ribbon of thickness d.

5.3 Simulation Examples

5.3.1 Magamp Simulation

The simulation model is based on the three-phase self saturating magamp as shown in Fig. 17, and is implemented in the dynamic simulation package Dymola [23], see Fig. 35.

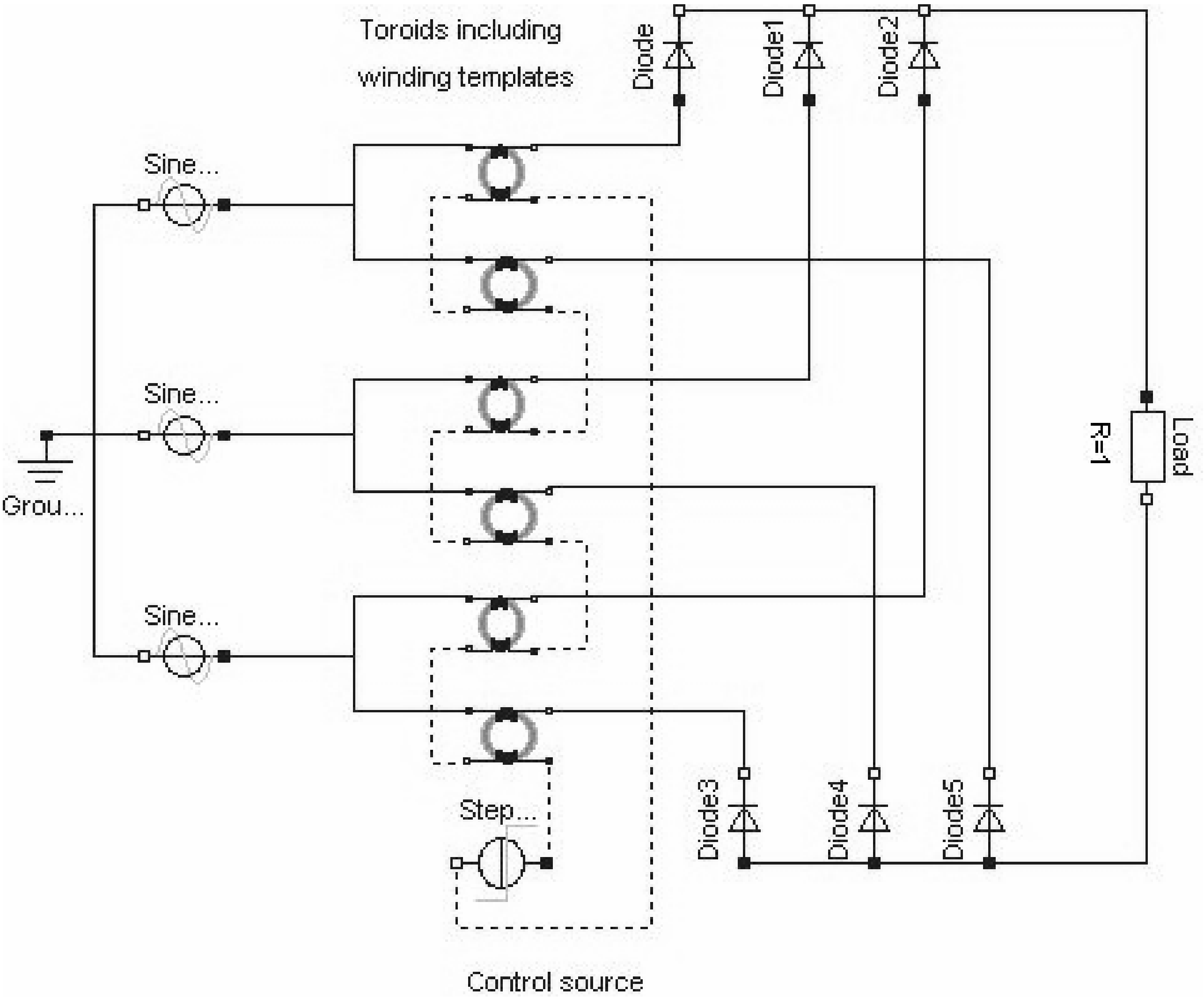

Fig. 35. Magamp simulation model

By adapting the factor GV_0 it is possible to obtain hysteresis curves that coincide fairly well with those given by the producer for Metglas 2605 TCA/S-2, see the dashed lines in Fig. 36.

Experimental data from the producer [19] is plotted as solid lines for DC, 60, 400 and 1000 [Hz].

The good compliance between experimental data and output from the model indicates a good potential for further improvements.

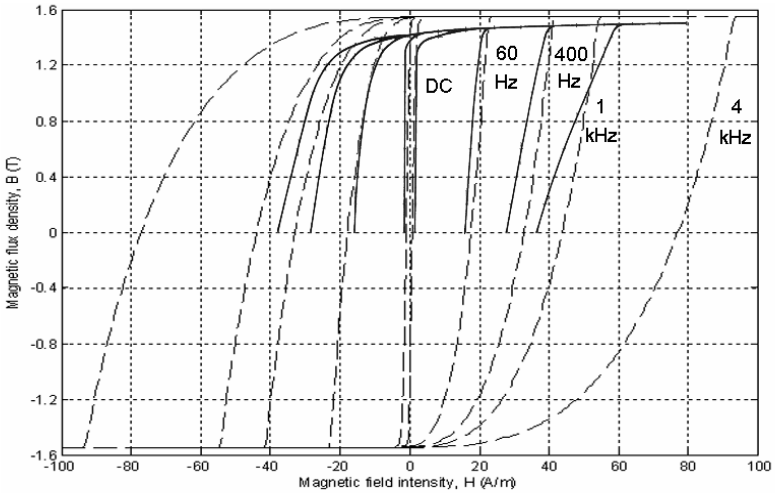

Fig. 36. Hysteresis model for Metglas 2605 TCA/S-2 Characteristics for different frequencies. The solid lines are the producers data, the dashed lines are major loops generated by the model.

The magnetization of the cores during operation in a three phase magamp application can also be analyzed by the model. Examples of simulated minor loops for different control currents are shown in Fig. 37.

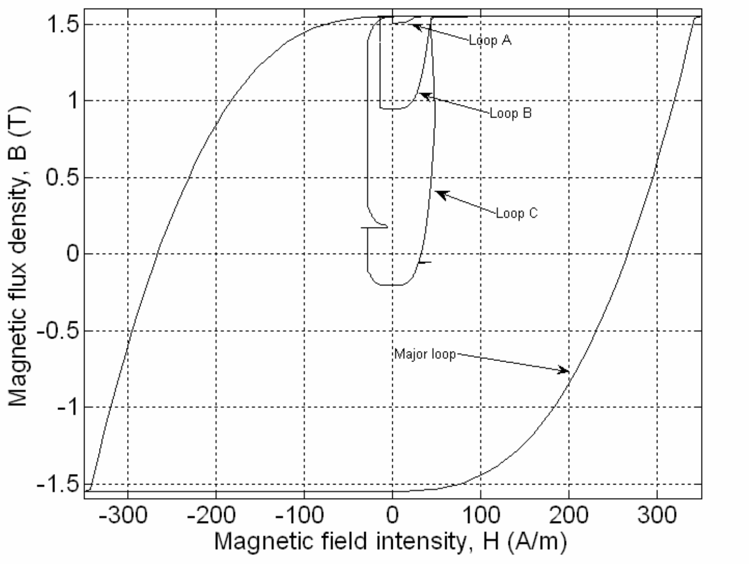

Fig. 37. Minor loop simulation at 4 kHz

Note that the major loop for 4 kHz, in Fig. 36 differs from that in Fig. 37. This is due to more rapid variations in the flux, corresponding to a higher magnetization field occurring in the application simulated and shown in Fig. 37.

5.3.1.1 The Magamp Losses

In the work presented in the thesis the efforts are concentrated on modeling of the core losses (the static hysteresis, the classical and the excess loss components), and the related copper losses in the power windings. The magamp as presented in Fig. 17 contains diodes and a control winding that also generates losses. Since the configuration of the magamp can differ, diode losses and copper losses in the control winding are not considered in this work.

5.3.1.2 The Core Losses

The simulation of the minor loops as shown in Fig. 37 represent typical features of the operation of a magnetic amplifier operating in a three-phase application according to a topology shown in Fig. 35.

The simulation of the circuit is performed at 4 [kHz], where each core constitutes a flux path length h =0.094 [m], an effective cross sectional area A=5.3 · 10^{-5} [m^2], a density ρ =7180 [kg/m^3], and a weight of 0.036 [kg]. The corresponding losses of the three loops A, B and C, are further analyzed in Fig. 38, 39 and 40. All loops are simulated for a supply voltage of 23 [V$_{\text{rms}}$] in each phase and a load R$_{\text{L}}$=1.156 [ohm]. The number of turns N_C in the control winding is 13.

The obtained loops are used when evaluating the core loss density given as [W/kg], according to Eq. (3.4).

Examples of simulation output of field quantities and losses are shown in Fig. 38, 39 and 40.

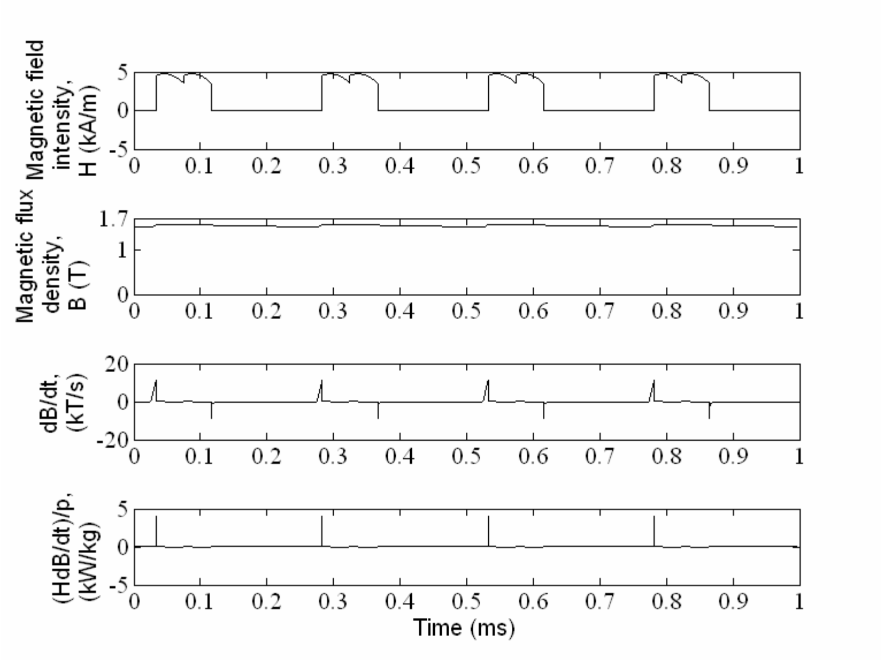

Fig. 38. Simulated field quantities and losses as functions of time for loop A

In loop A with I_C=0 [A], the magamp operates at a power output of 1200 [W]. The corresponding core loss density then is 0.73 [W/kg] giving P_{Acore}= 0.026 [W]. Note the high H-field due to saturation of the core, during the conducting phase of the magamp.

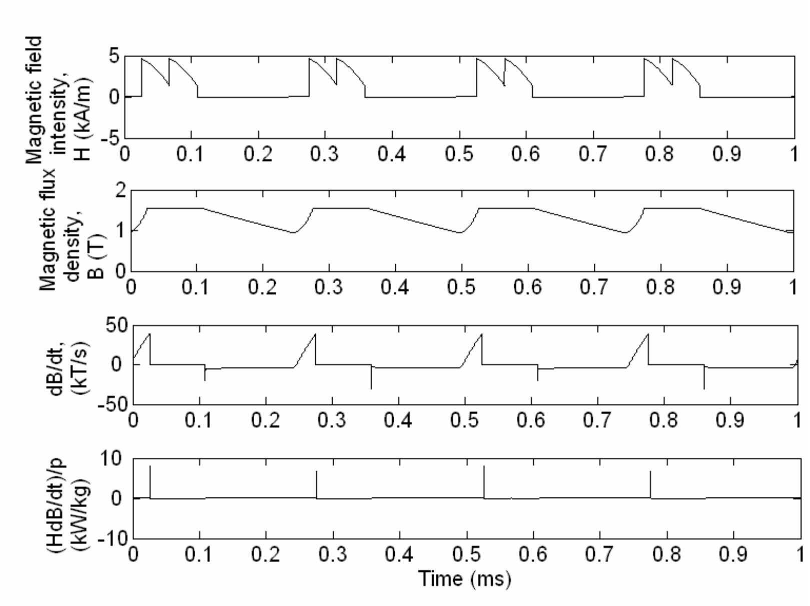

Fig. 39. Simulated field quantities and losses as functions of time for loop B

In loop B with I_C=0.1 [A], the magamp operates at a power output of 730 [W]. The corresponding core loss density then is 15.3 [W/kg] giving P_{Bcore}= 0.55 [W].

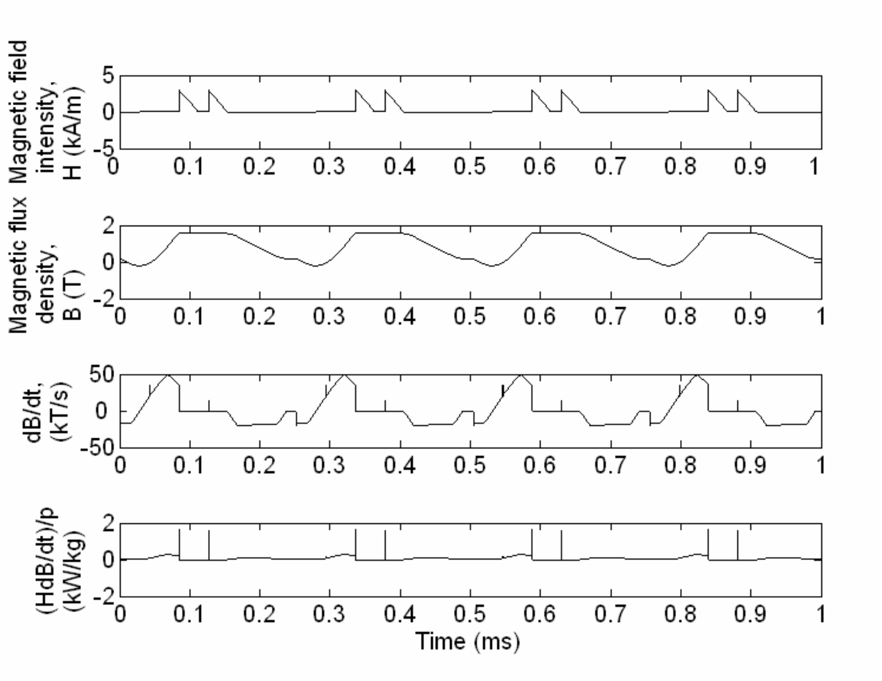

Fig. 40. Simulated field quantities and losses as functions of time for loop C

In loop C with I_C=0.2 [A], the magamp operates at a power output of 130 [W]. The corresponding core loss density then is 60.8 [W/kg] giving P_{Ccore}= 2.18 [W].

5.3.1.3 The Copper Losses in the Power Winding

The copper losses in each core are calculated according to:

$P=R \cdot I^2/p$ where $R=\rho_{Cu} \cdot k \cdot l \cdot N/A_{Cu}$

p	is the number of phases
k	is a factor for skin effect (set to 1 in this example)
l	is the length of each turn [m]
N	is the number of turns

A_{Cu} is the cross sectional area of the copper wire [m^2]

ρ_{Cu} is the resistivity of $2.15 \cdot 10^{-8}$ [ohm⋅m] when operating at a temperature of 85 [°C].

The copper losses are P_{ACu}= 0.73 [W], P_{BCu}= 0.44 and P_{CCu}= 0.08 [W] respectively, given by the simulations where p=3, l=0.047 [m], N=13, $A_{Cu} = 5 \cdot 10^{-6}$[m].

5.3.1.4 The Magamp Efficiency

In the simulated examples, the magamp in Fig. 38, 39 and 40 is operated at 1200 [W], 730 [W] and 130 [W] for loop A, B and C respectively. The simulations yield the total losses of each core $P_A=P_{Acore}+P_{ACu} =$ 0.76 [W], P_B= 0.99 [W] and P_C= 2.26 [W], for loop A, B and C respectively.

The efficiency, defined as the input power minus the losses of six cores divided by the input power, gives an efficiency of 99.6 %, 99.2% and 90.6 % for the magamp operating at loops A, B and C respectively.

5.3.1.5 Detailed Simulation

The so far performed simulations are done on the three-phase self saturating magamp shown in Fig. 17, The control current, I_C, has been 0, 0.1 and 0.2 A i.e. zero control current or a positive control current taking the core out of saturation.

This detailed simulation will be the reference and compared with tests performed with negative control currents in section 5.4.1.6.

Initially a detailed simulation with zero control current i.e. I_C=0 mA is performed, shown in Fig. 41 where details of the minor loop can be studied. The examples shown in Fig. 41, 42 and 43 shall only be compared with each other.

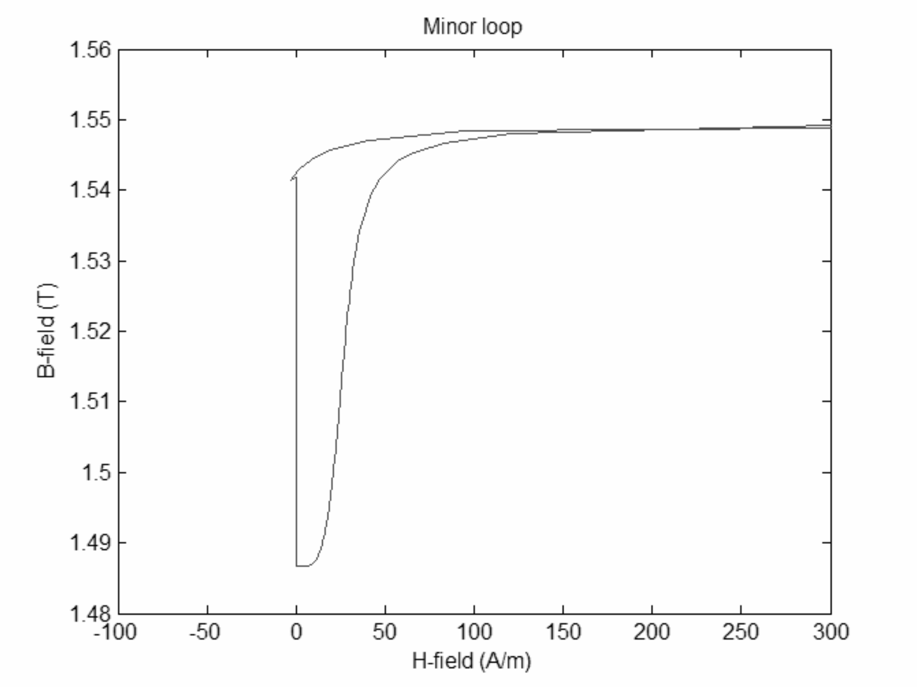

Fig. 41. A detailed simulation with a control current of I_C =0 mA

In the detailed simulation of a loop A shown in Fig. 41, with I_C=0 [A], the magamp operates at a power output of 1184 [W]. The corresponding core loss density then is 3.1439 [W/kg] giving P_{Acore}= 0.1132 [W]. Note the high H-field due to saturation of the core, during the conducting phase of the magamp. Copper losses P_A in the power winding is 0.73 [W].

The difference between loops A as presented in Fig. 37 and Fig. 41 showing higher iron losses in the detailed simulation. The difference can be explained by that the simulation is performed with different resolution and the fact that the impact of the short duration on the contribution to the losses expressed by dB/dt in equation (5.11) will be sensitive to how detailed the simulation is.

5.3.1.6 Detailed Simulation with Negative Control Current

The intention of the detailed simulations is to more thoroughly investigate the hysteresis loops. The impact of changing the polarity of the control current, which will result in further saturation of the cores, is here subjected to detailed studies of the hysteresis loops.

A simulation with a control current I_C of -50 mA was performed, with a deeper saturation than in Fig. 41. The simulation result is shown in Fig. 42.

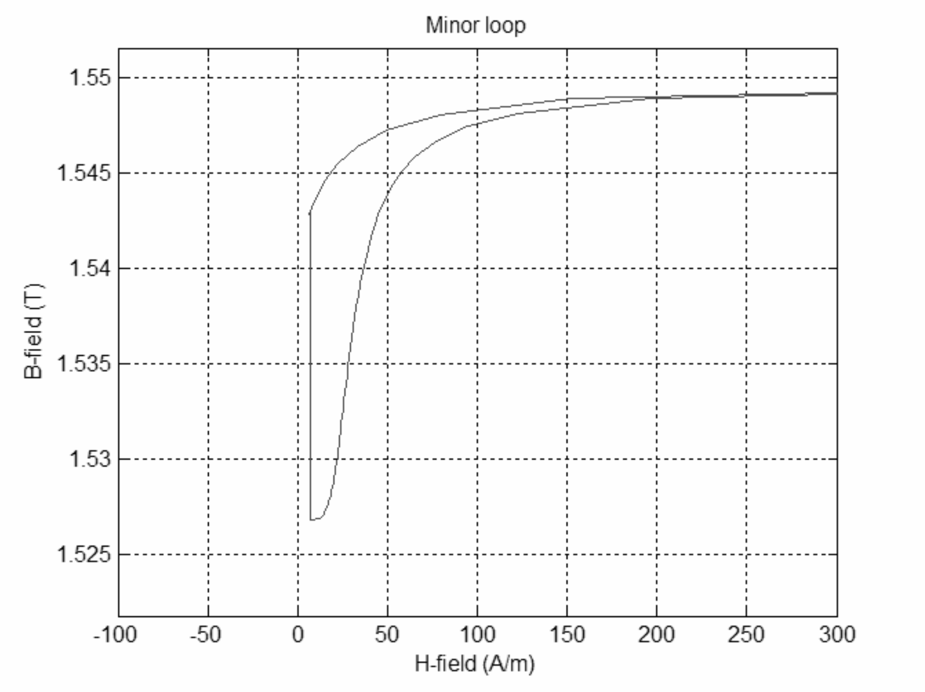

Fig. 42. A detailed simulation with a control current I_C of -50mA

In the detailed simulation with a control current I_C of -50 [mA], the magamp operates at a power output of 1222 [W]. The corresponding core loss density was 1.5174 [W/kg] giving P_{Acore}= 0.0546 [W]. Note the high H-field due to saturation of the core, during the conducting phase of the magamp. The copper losses in power winding is slightly increased due to an increased power output and equal to P_A =0.74 [W].

An additional simulation with even deeper saturation using a control current of -100mA was performed and is shown in Fig. 50. The control current then supports the saturating in the cores even more, resulting in even lower losses.

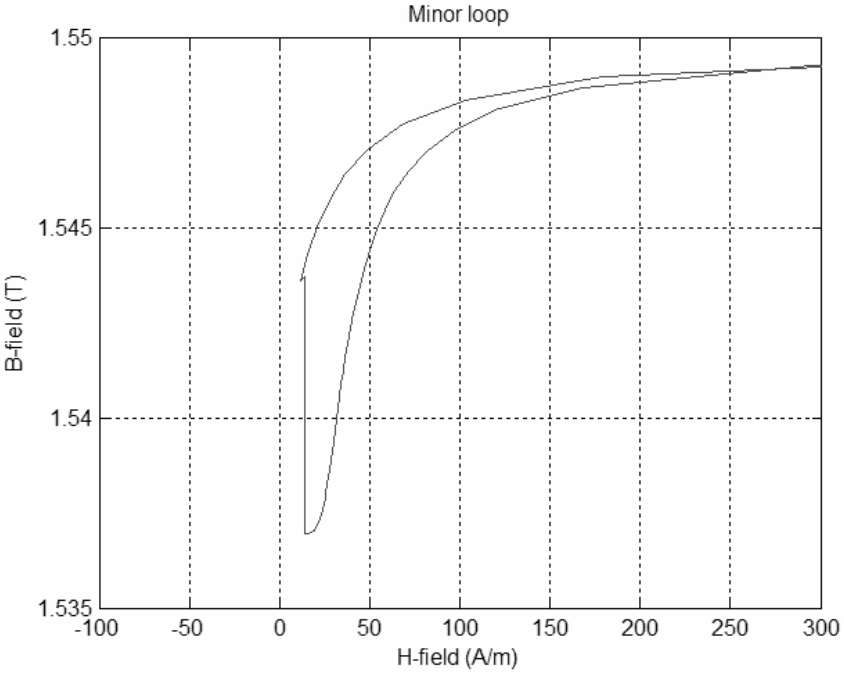

Fig. 43. A detailed simulation with a control current I_C of -100mA

In the detailed simulation with a control current I_C of -100 [mA], the magamp operates at a power output of 1231 [W]. The corresponding core loss density was 1.1328 [W/kg] giving P_{Acore}= 0.0408 [W]. The copper losses in power winding was slightly increased due to an increased power output and equal to P_A =0.75 [W].

With a control current I_C of -100 [mA] the saturation will be deeper. Note that the hysteresis loop will not cross the y-axis with zero magnetic field. The minimum magnetic field will then depend on the control current.

With the used parameters the corresponding minimum H-field can be calculated. The length of the flux path length h_{Fe} =0.094 [m], and the number of turns N_C in the control winding is 13.

This gives

$$H \cdot h_{Fe} = N_C \cdot I_C$$

and

H=13 · 0.1/0.094= 13.8 [A/m],

which is a result that complies with the simulation shown in Fig 43.

The examples in Fig. 42 and 43 indicate that saturation control can further improve the efficiency, with reduced core losses, as well as increased output power of the magamp. With a control current that saturates the core the magnetic field remains positive during the complete hysteresis loop. The examples shown in Fig. 41, 42 and 43 shall only be compared with each other.

5.3.1.7 Output Power Characteristics

The output power characteristics can be evaluated for a typical output of the three-phase magnetic amplifier according to the presented simulation model in Fig. 35. In Fig. 44 it can be seen how the sum of the output from the six switches after filtering gives an average of 730 [W] for loop B, presented in Fig 39.

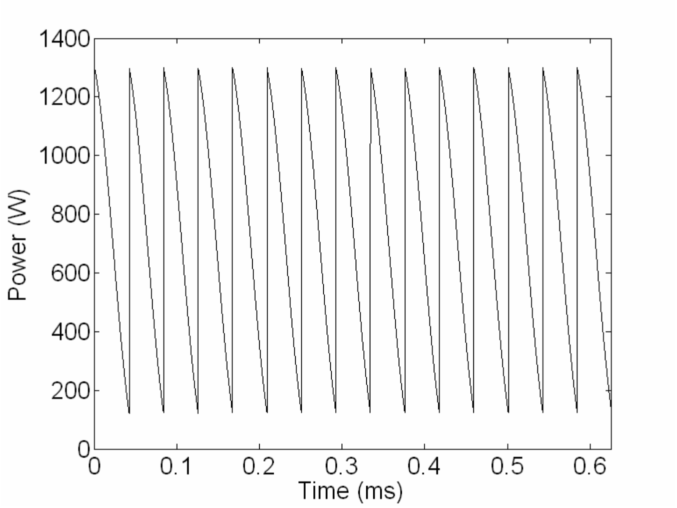

Fig. 44. Output power characteristics corresponding to loop B

5.4 Analysis of Losses and Weight of a Magamp Core

The iron losses per kilo can be described as a function of frequency and peak flux density, $\hat{B}$. In evaluation of the iron losses in a magamp application, with unsymmetrical flux, the peak flux density is half of the peak to peak value of the flux.

Eq. (5.13) constitutes such an empirical function is given by Metglas [19] for the amorphous material 2714A.

$$P = 9.93 \cdot 10^{-6} \cdot f^{1.57} \cdot B^{1.7} \tag{5.13}$$

For the material 2605TCA the core losses are graphically given in Fig. 22 by the manufacturer. The Eq. (5.14) is extracted, based on these graphs.

$$P = 88 \cdot 10^{-6} \cdot f^{1.57} \cdot B^{1.7} \tag{5.14}$$

,which yields good compliance with data in Fig. 22 up to 10 000 Hz. These losses also are showed to be approximately 9 times bigger than those obtained from equation (5.13).

The weight of the core is:

$$m = h_{Fe} \cdot A_{Fe} \cdot \rho \tag{5.15}$$

where h_{Fe} is the average iron flux path length, A_{Fe} the average core cross sectional area and ρ is the density of the different alloys:

2714A ρ=7590 kg/m^3

2605TCA ρ=7180 kg/m^3

The relation between number of turns, N, and the average core cross sectional area, A_{Fe}, is given in equation (5.16). The parameters such as peak flux density $\hat{B}$, voltage, E, and frequency are given by the operational requirements.

Fel! Objekt kan inte skapas genom redigering av fältkoder. (5.16)

Note for square wave applications the factor 4.44 is changed to 4.00.

The frequency can be described in terms of the period time *T*. The voltage-time product $U \cdot T$ is calculated.

$$U \cdot T = 2 \cdot B \cdot A_{Fe} \cdot N \tag{5.17}$$

The flux density span is 2B, because the flux can be used over the whole span from negative to positive B.

5.4.1 Graphical Analysis Example

In Fig. 45 a graphical example is given for a three phase magamp, designed for an output power of 10 000 W, with an output voltage of 270 VDC. The core losses are estimated by equation (5.14), and the weight by equation (5.15).

The graph is based on different number of turns, N. The resulting core losses are calculated for different core cross sectional areas, A_{Fe}, see Eq. (5.17). The corresponding core weights are shown in the figure.

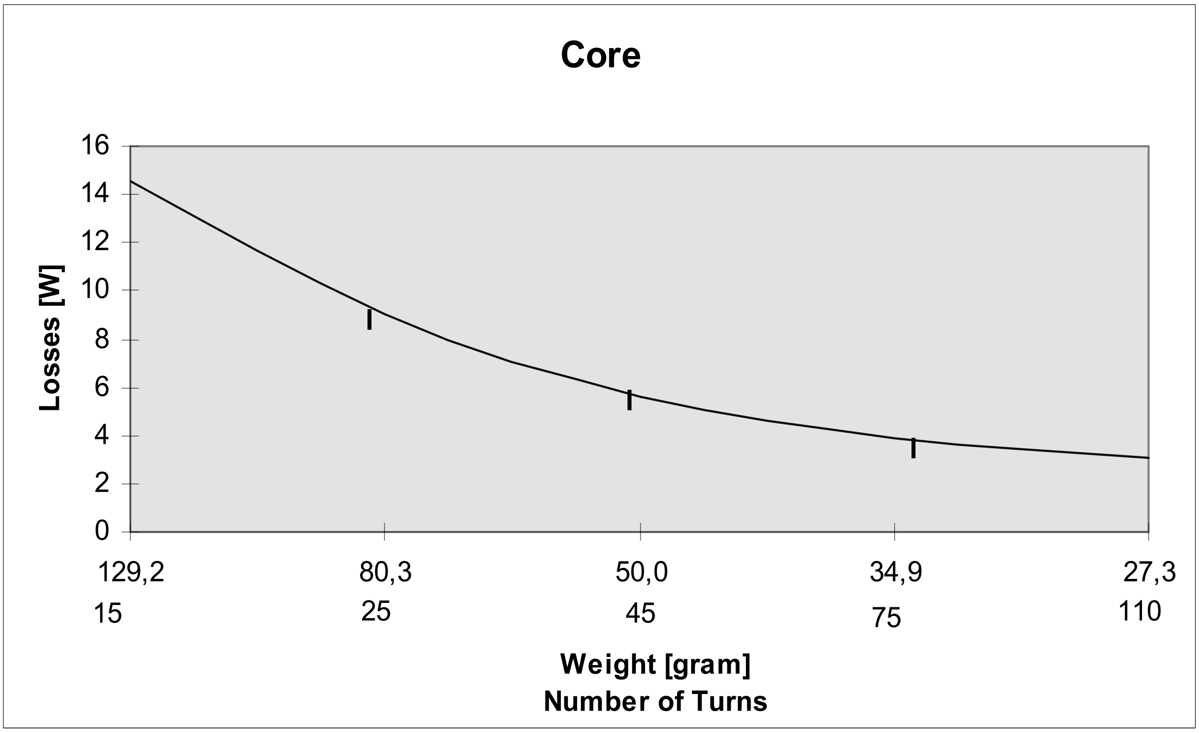

Fig. 45. The core losses for 2605TCA

5.4.1.1 Geometric Core and Copper Data

In the previous example, the chosen material and the related maximum flux density, and the needed core area A_{Fe} can be calculated by use of Eq. (5.18)

For a given number of turns *N* the corresponding required core area then is:

$$A_{Fe} = U \cdot T \big/ N \cdot 2B \tag{5.18}$$

Length of Copper Wire per Turn

The performed analysis, assumes a square core cross section, but is not limited to any standard selection. The calculation of the length of the copper wire will be based on the core area. The average turn length will be calculated as the sum of the length of the inner turn and the length of the outer turn divided by 2. The encapsulation of the core is estimated to add a total of 10 % of the inner turn length. This represents a factor of *c*=1.1, however this factor *c* can vary depending on type of encapsulation.

The inner length then is $\sqrt{A_{Fe}} \cdot (4 \cdot c)$

4 is the number of sides and *c* represents the margin of encapsulation.

At a winding window utilization factor of 30% the inner diameter of the winding d_w can be calculated according to

$$(\pi/4)d_w^2 = (\pi/4)d_i^2\,(1-0.3) \qquad \Rightarrow \quad d_w = 0.8366\, d_i$$

,where d_i is the core inner diameter without encapsulation, see Fig. 46.

The outer length now can be expressed as $4\left(\sqrt{A_{Fe}} + 2d_i(1-0.8366)\right)$

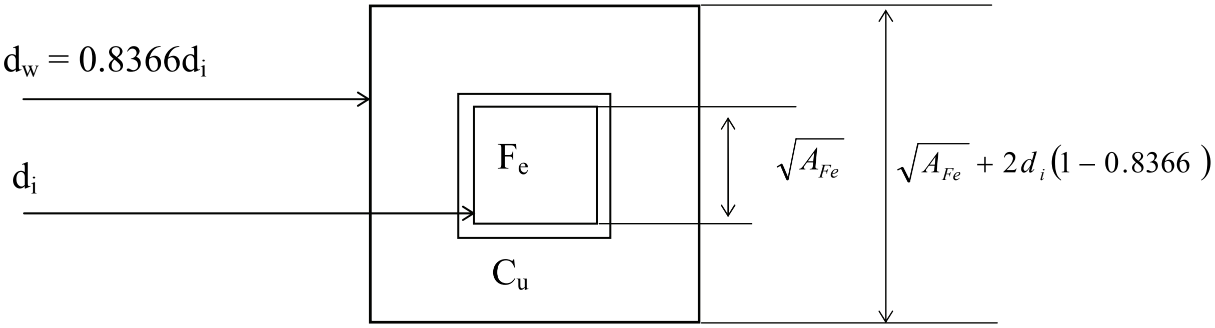

Fig. 46. The copper winding, cross section.

With *c*=1.1 the average turn length will be:

$$l_{Cu} = \left(\sqrt{A_{Fe}} \cdot (4 \cdot 1.1) + 4 \cdot \left(\sqrt{A_{Fe}} + 2d_i(0.1634)\right)\right)/2$$

$$l_{Cu} = \sqrt{A_{Fe}} \cdot 4.2 + d_i \cdot 0.1634 \cdot 2 \qquad (5.19)$$

5.4.1.2 Copper Losses

The copper losses are basically depending on the current, the turn length, number of turns and the copper area A_{Cu}. The wire length is calculated by use of the average length per turn, that gives the resistance according to:

$$R = \rho \cdot k \cdot l_{Cu} \frac{N}{A_{Cu}} \quad \text{, where} \tag{5.20}$$

$\rho = 2 \cdot 10^{-8}$ ohmm at 85 °C

k is the skin factor. At higher frequencies k>1.

For details about the skin factor, see section 6.2.1. It can be noted that there is a very low impact of the skin effect (less than 10%) for a wire of a diameter less than 2 [mm] as long as the frequency is less than 10000 Hz.

The copper losses are: $P_{Cu} = R \cdot I^2 / n$ (5.21)

where n is equal to 2, due to the 50 % duty cycle, for a 1 phase magamp and 3 for a 3 phase magamp, and in all other cases n complies with the number of phases.

Weight of Copper Wire

The weight of the copper wire is:

$$m = l \cdot N \cdot A_{Cu} \cdot \rho \tag{5.22}$$

where ρ =8900 [kg/m^3]

The copper losses given by Eq. (5.21) and corresponding copper weight given by Eq. (5.22) are shown in Fig. 47 for N given as 15, 25, 45, 75 and 110 turns.

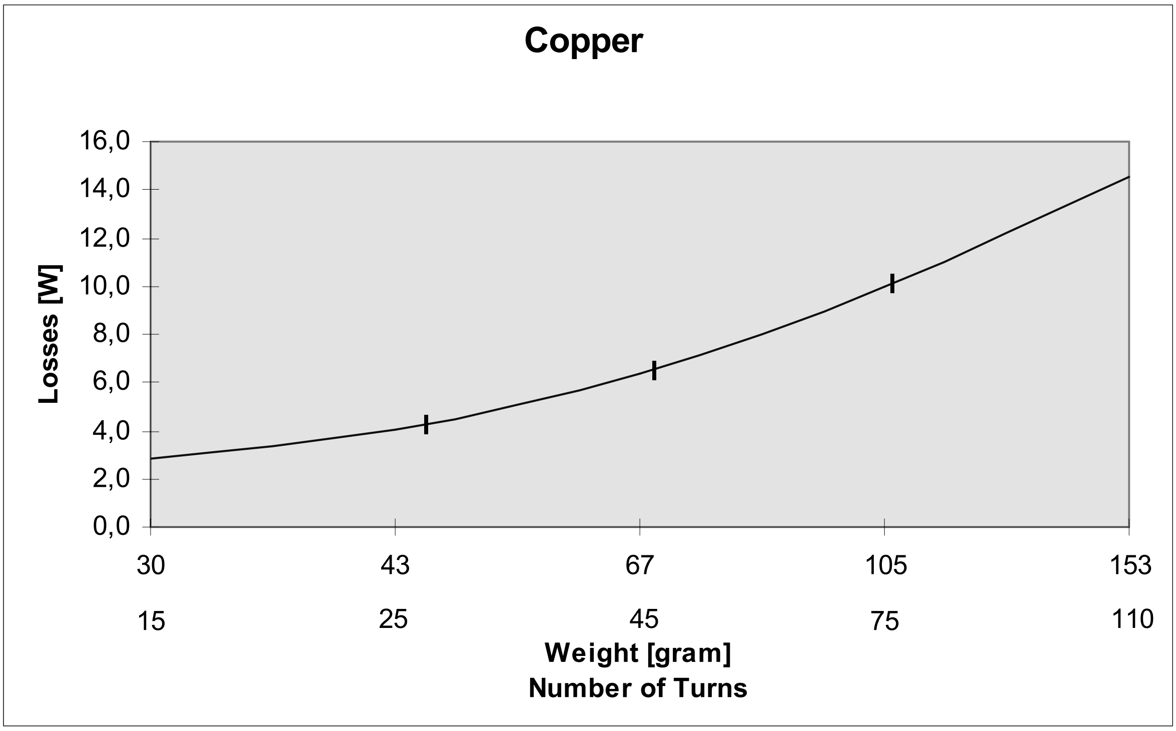

Fig. 47. The copper losses

5.4.1.3 The Total Losses

It can be noted that the core losses is decreasing for a higher number of turns, N, while the copper losses is increasing. One ambition is to find a way of minimizing the weight and losses. In Fig. 48 the sum of core and copper losses $P_{total}=P_{Fe}+P_{Cu}$ is studied and is shown as a function of the total weight for alternative windings with different number of turns N. It can be noted that the lowest weight case coincides with the lowest losses case in the presented example.

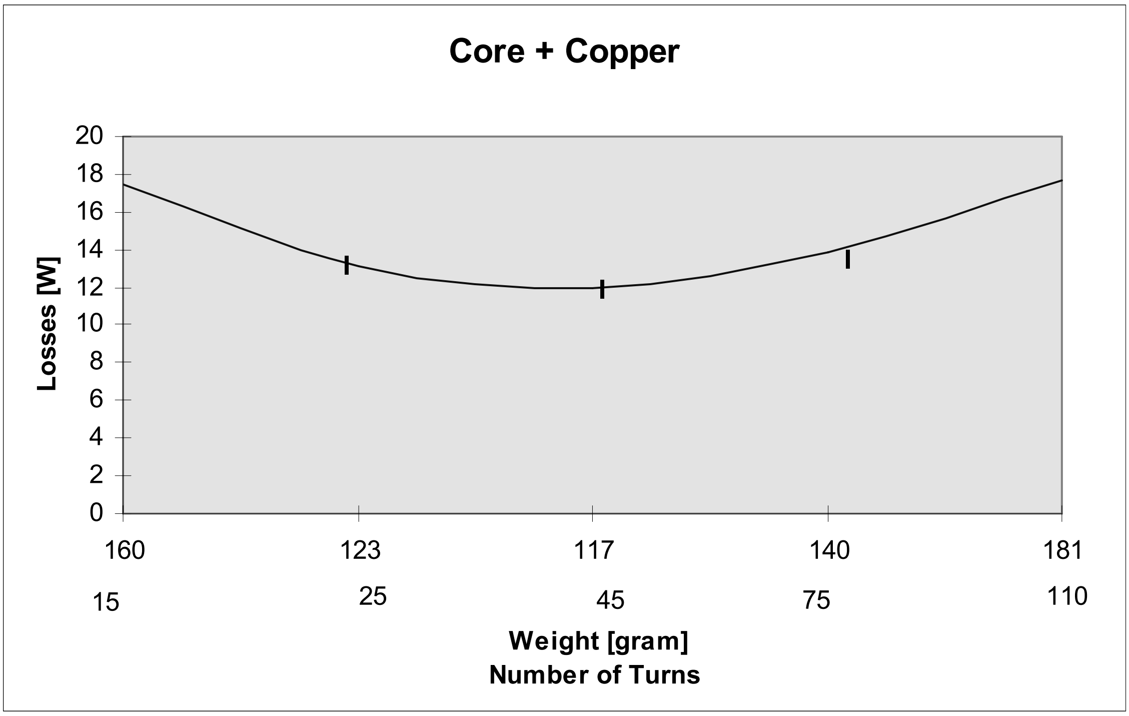

Fig. 48. The core and copper losses

5.5 A Proposed Engineering Tool

The proposed engineering tool offers a quick method of analyzing whether a magamp design is possible for a considered application. Weight and efficiency are parameters that are analyzed by the proposed tool. In aircraft design, information regarding e.g. frequency and weight must be communicated between system design [3] and component design groups. This can be accomplished by this engineering tool.

The methodology of analyzing the weight losses in a magamp is demonstrated by:

1. Specify power requirement, output current and voltage

2. Specify number of phases

3. Choose alloy for the cores, and specify max flux density

4. Choose copper area

5. Choose insulation factor

6. Make a preliminary choose of core inner diameter

7. Make a preliminary set up of the number of turns

8. Evaluate graphically given results

The tool automatically calculates iron and copper losses and iron and copper weights given as a function of the given set of turns of the power winding. The winding window utilization factor will automatically be calculated; in this thesis 30 % is used, but can be higher or lower. During the design evaluation in step 8, any of the inputs in step 1-7 can be varied until the magamp meet the design goals, or the best possible compromise is achieved.

The optimization of the magamp can be slightly different depending on the load profile, i.e. whether the magamp is mostly on or off. In an initial study it can be sufficient to look at the sum of the core and copper losses.

Other features as required core size and control current and number of turns are important [33]. As a general rule, the design shall utilize a minimal amount of core material that implies low weight and losses.

Feature

The tool estimates output data like weight, dimensions and losses based on defined equations and input data. In similarity with a transistor circuit the magamp must be designed to meet the requirements of current as well as voltage. The difference is that the voltage capability of the magamp is in terms of volts during a period of time [Vs].

Usage

Numbers of turns are used as an input parameter. Selections of different number of turns N are used to evaluate weight end losses. The tool gives an opportunity to evaluate weight end losses for different N. It will support the design optimization process, by graphically showing where one can find the minimum weight and losses.

The skin factor, see section 6.2.1, has been included in the tool, where the wire diameter and the frequency is used to automatically calculate the resulting winding resistances that are included in the tool.

Note that the design tool does not include any design margins with respect to e.g. tolerances in area and material, as well as design margins normally considered due to variations in temperature and aging. Furthermore the engineering tool will not treat the losses in diodes and the control circuit.

5.5.1 Input Parameters

Typical input specification-data can be as in table 3. Core inner diameter d_i [mm] specifies the core without encapsulation. When choosing the wire cross sectional area the current density [A/mm^2] must be considered with respect to cooling capability. In our examples 6.5 [A/mm^2] is chosen, which requires cooling. The insulation factor *c* is an input parameter, see section 5.4.1.1.

In the calculations a winding window utilization factor of 30 % is used.

Table 3. Examples of input parameters

Input Parameters	
Current [A]	37
Voltage [V]	270
Frequency [Hz]	5000
Phases p	3
Alloy	2605TCA
Flux B [T] (Peak value)	1,5
Area A_{Cu} [mm^2]	3,3
Turns N	45
Core d_i [mm]	45
Winding window utilization factor %	30
Insulation factor *c*	1.1

From the given input parameters an Excel program can perform the calculations and present output parameters and graphs to support a design decision.

5.5.2 Dimensioning-Calculation Examples

A feasible aircraft application can be a converter for 270 VDC, at a power level of 10 kW. A few cases with different input data are studied.

The purposes of the studied cases are to investigate whether a design can be optimized, such that weight and losses can be minimized in the same design.

In the process of evaluating the engineering tool, four cases of a three phase magamp applications are presented and shown in cases 2, 3, 4 and 5, case 2-5 is shown in Fig. 49, 50, 51 and 52. Case 1 is a one phase application based on a Ramey amplifier, presented in Table 5.

The corresponding data to the studied cases are presented in Table 4. The graphs for minimization of losses and weight are shown in Fig. 49, 50, 51 and 52.

In the following cases, two different alloys are studied at different frequencies.

The case shown in Fig. 49 is based on the alloy 2605TCA indicates that an optimization of the design for the chosen performance can be achieved at 5000 Hz. The design show coinciding weight and loss minimization. The following cases are studied:

Table 4. Cases studied

Case	Alloy	Freqency	Phases	Fig. no.
1	2605TCA	5000	1	NA
2	2605TCA	5000	3	49
3	2605TCA	10000	3	50
4	2714A	5000	3	51
5	2714A	90000	3	52

A number of calculations have been performed with different input parameters, giving the outputs that can be seen in Table 4. The circuits studied in case 1 can be seen in Fig. 14, and the circuit used in case 2-5.

It is of special interest to study the total weight, the losses and the efficiency. In the cases 2-3, Fig. 49 and 50, it can be noted that the losses show minimum at the same number of turns (N=45). The weight and losses coincides with a minimum at N=45 in case 2 shown in Fig.49.

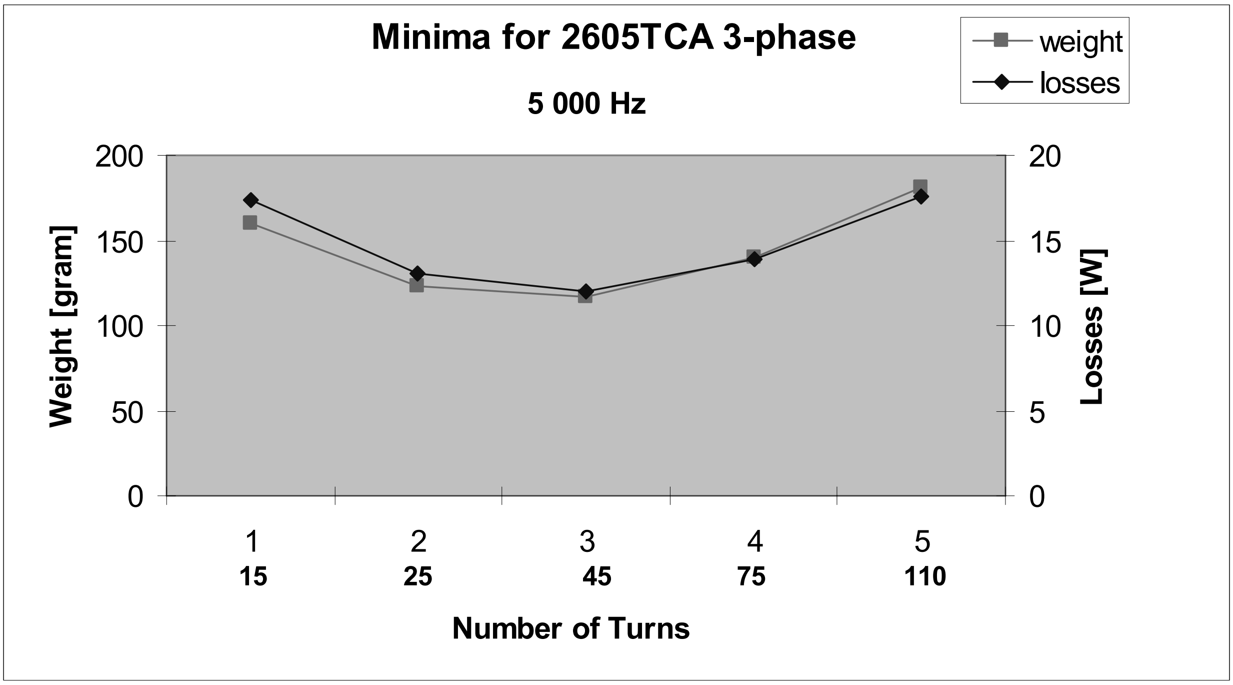

Fig. 49. Case 2 giving coinciding minimum

The total losses for the six cores are 6 · 12 =72 [W] and the weight is 6 · 117=702 [g] at N=45 in case 2, Fig. 49.

At a frequency of 10000 Hz, shown in case 3, Fig. 50, it can be noted that that the minimum regarding weight and losses do not fully coincide.

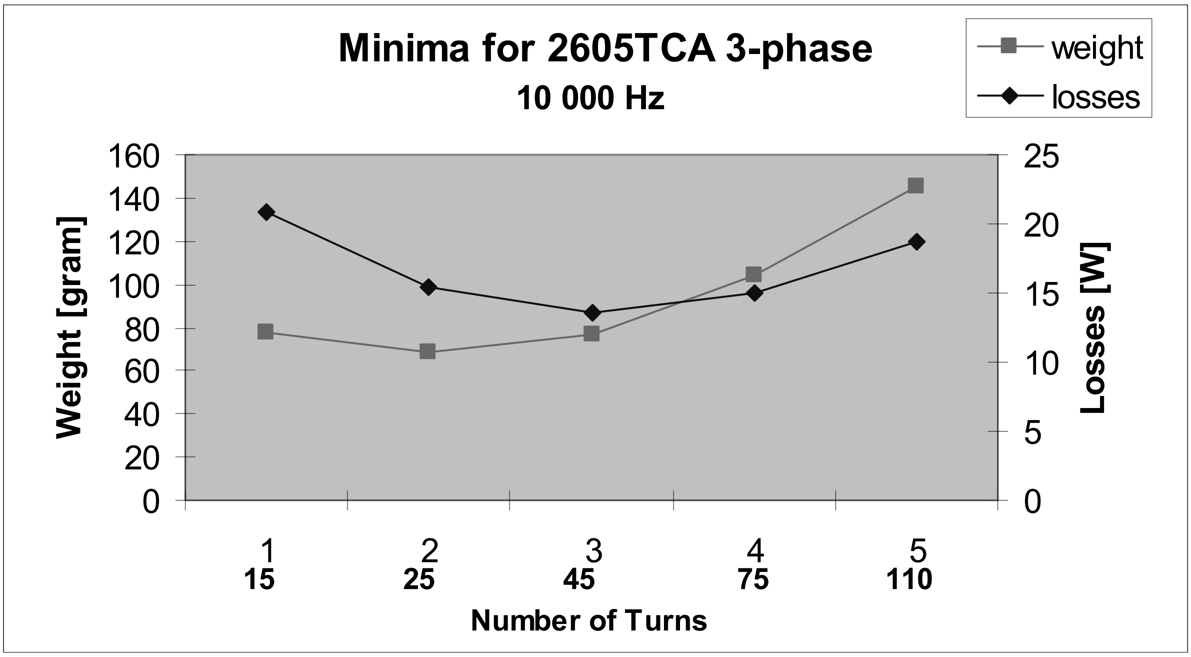

Fig. 50. Case 3 giving split minimum

The total losses for the six cores in case 3 are 6 · 13.5=81 [W] and the weight is 6 · 76.8=460.8 [g] at N=45 in case 3, Fig. 50. The weight could be reduced to 6 · 68.6=411.6 [g] at N=25 giving higher losses of 6 · 15.5=93 [W]. The lower minimum weight can be explained by the increased frequency. In case 3, Fig. 50, Table 4, it can be noted that the doubled frequency (10 [kHz]) is giving a total weight of only 6 · 76.8=460.8 [g].

With full advantage of the increased frequency, a weight of approximately 6 · 50=300 [g] could be achieved when the current density is doubled. This might be a bit unrealistic. In our example the current density is kept at 6.5 [A/mm^2].

For the alloy to 2714A, and 5000 Hz it can be noted that the minima for weight and losses do not coincide, see case 4, Fig. 51.

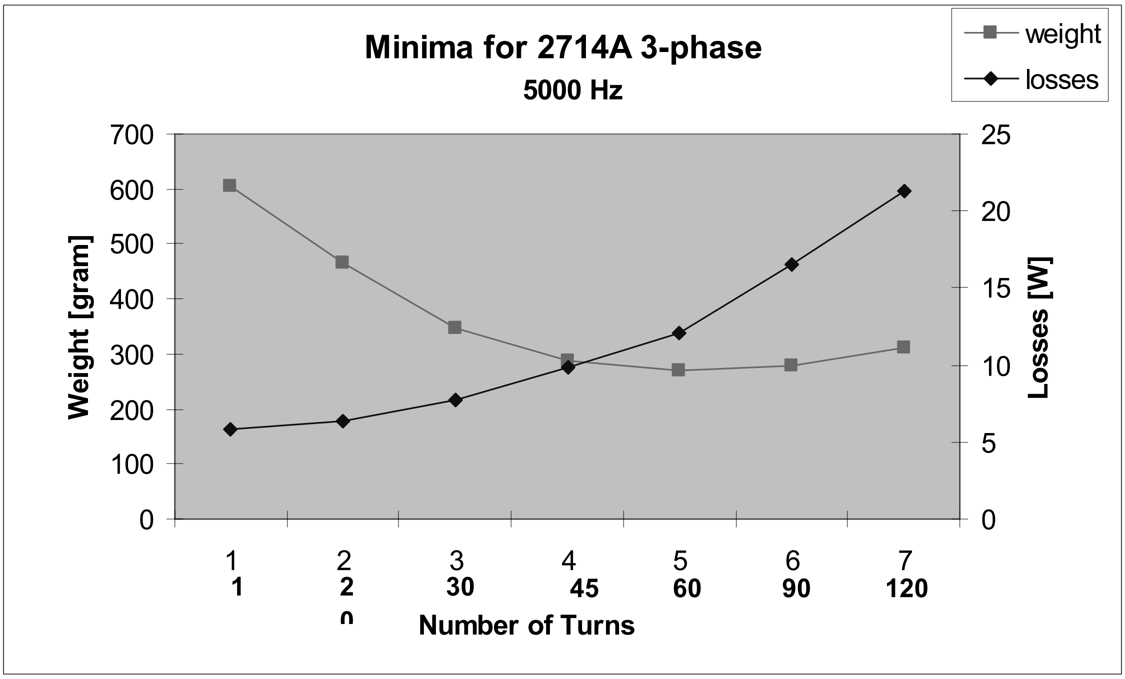

Fig. 51. Case 4 giving of split minima

This represents a compromise with the total losses for the six cores of 6 · 9.9=59.4 [W] and a weight of 6 · 286.7=1720.2 [g] at N=45 as shown in case 4, Fig. 51, with a potential for further reduced losses at a higher weight.

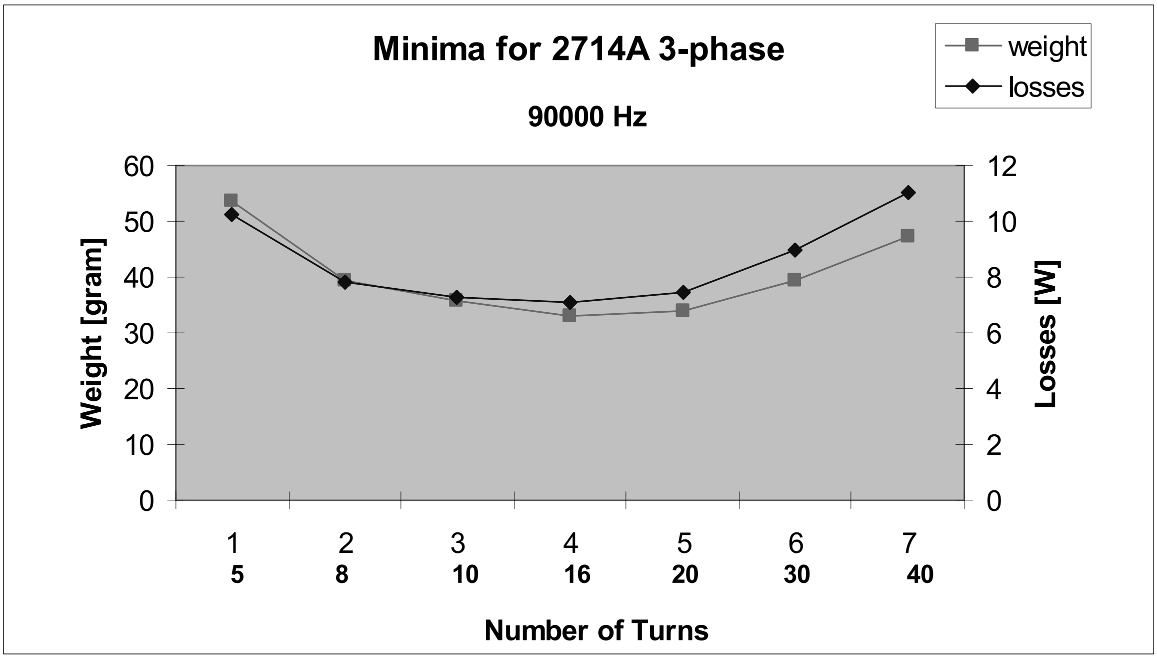

Fig. 52. Case 5 giving coinciding minima

The losses, referred to in case 4, Fig. 51, can be reduced to 6 · 7.1=42.6 [W], in case 5, Fig. 52, at a weight decreased to 6 · 33=198 [g] in an application working with 90 kHz where the minimum for weight and losses coincide better, at N=16, see case 5, Fig. 52. Note that the high frequency involves design concerns such as skin effect.

Table 5. Examples of output data from the engineering tool for different sets of input parameters

Magamp Case	1	2	3	4	5
Fig.		Fig. 49	Fig. 50	Fig 51	Fig. 52
Current [A]	37	37	37	37	37
Voltage [V]	270	270	270	270	270
Frequency [Hz]	5000	5000	10000	5000	90000
Phases p	1	3	3	3	3
Alloy	2605	2605	2605	2714	2714
Flux B [T]	1.5	1.5	1.5	0.5	0.5
Area A_{Cu} [mm^2]	8	3.3	3.3	3.3	3.3
Turns N	50	45	45	45	16
Core d_i [mm]	41	25	25	25	17
Outer d [mm]	58	35.2	32.8	41.2	23.4
Height [mm]	20	12.2	9.9	18.2	8.4
Volume [mm^3]	52690	11920	8332	24266	3593
Weight [g]		117	76.8	286.7	33
Total weight [g]	470	700.2	460.8	1720.2	198
Total power [W]	9990	9990	9990	9990	9990
Output/core [W]		1665	1665	1665	1665
Losses/core [W]		12	13.5	9.9	7.1
Total losses [W]	49	72	81	59.4	42.6
Losses %	0.5	0.72	0.81	0.6	0.42
Efficiency %	99.5	99.28	99.19	99.4	99.58

5.5.3 Preliminary Interpretations of the Results from the Engineering Tool

The use of the engineering tool indicates that for a given power rate an optimized design, with minimized losses can be achieved by minimizing the weight of the core, by choosing the operation frequency and a suitable alloy for the core, as shown in case 2 and 5, Fig. 49 and 52.

The advantage of a design with the alloy 2605TCA at e.g. 5000 Hz, is that the lowest losses coincide with the lowest weight. The thesis that the iron losses is in proportion to the mass of iron is valid in a magamp application designed to use largest possible flux. The demonstrated optimizations seem to be valid for different cases where the same flux level occurs. The losses can be lowered by using a smaller proportion of the available flux swing, but the consequence then is increased weight.

The study indicates that the lowest losses coincide with the lowest weight the losses in the core are about equal to the losses in the copper wire. This can be seen in the cases 2 and 5, shown in Fig. 49 and 52.

It can be noted that the higher the flux density, the lower the weight can be.

This is indicated in case 2, Fig. 49, with an alloy with a max flux density of 1.5 T that yielded a weight of $6 \cdot 117=702$ g. In case 4, Fig. 51, with an alloy with a max flux density of 0.5 T the weight was indicated to be $6 \cdot 286.7=1720.2$ g.

These examples are identical except for that the used alloys admit different flux densities.

The efficiency of the magnetic amplifiers is estimated to be as high as 99.3 % and the corresponding power-density then easily can meet 14 [kW/kg] in the 5000 [Hz] application.

The conclusion is that a core in the 2605-family is the preferable alloy for audio frequencies, due to the possibility to achieve a design with low weight and thus achieve low losses. The 2714A alloy might be preferable in the 90 kHz range, with a potential of efficiency near 99.6 %. At this frequency the skin effect, however, has increased the resistance that increases the losses, and reduces the efficiency. This problem could be corrected by splitting the current in a number of parallel wires.

5.6 Conclusions

The proposed simulation model approach is considered to be a feasible tool in the design of magnetic amplifiers. This means that the modeling approach can be used to evaluate magnetic and resistive losses of tentative magnetic amplifier designs.

The engineering tool appears to be a useful tool in the initial stage of a design.

Both the proposed simulation model and the engineering tool need further development. Experimental verifications of the models with electric and/or calorimetric methods remain.

Chapter 6

System Integration in Aircraft Applications

6.1 Aircraft Power Supply Systems

In the process of designing an aircraft power supply system, specific attention must be paid to low weight and high reliability. A conventional system is specified by Mil-Std-704E, which stipulates 28VDC, 200/115VAC, 400Hz or 270VDC systems.

It is of vital importance to find the optimal concept for the power supply in future designs, where power levels of 1 MW installed power is indicated in civil aircrafts. In military aircrafts a significant increase in power levels can be foreseen due to the more electric aircraft technology concepts include electric actuation, electric cooling systems, electric motor start systems and electric weapon systems. Variable frequency power supply systems are used in e.g. Saab 2000 and have been proven to be a good design.

In Saab JAS39 Gripen the power supply of the electronic flight control system is based on a generator giving variable frequency (2400-4000Hz) and variable voltage. The PM-generator in JAS39 Gripen is an 18-pole generator operating up to 26 666 rpm. The power rating is approximately 2000W. The generator is shown in Fig. 53. A total of 27 teeth can be seen on the Saab stator windings. Behind the Saab windings the stator for supply of the engine control can be seen. The rotor can be seen in Fig. 54. Note the two rotor packages with the permanent magnets. The permanent magnets are encapsulated by stainless steel rings.

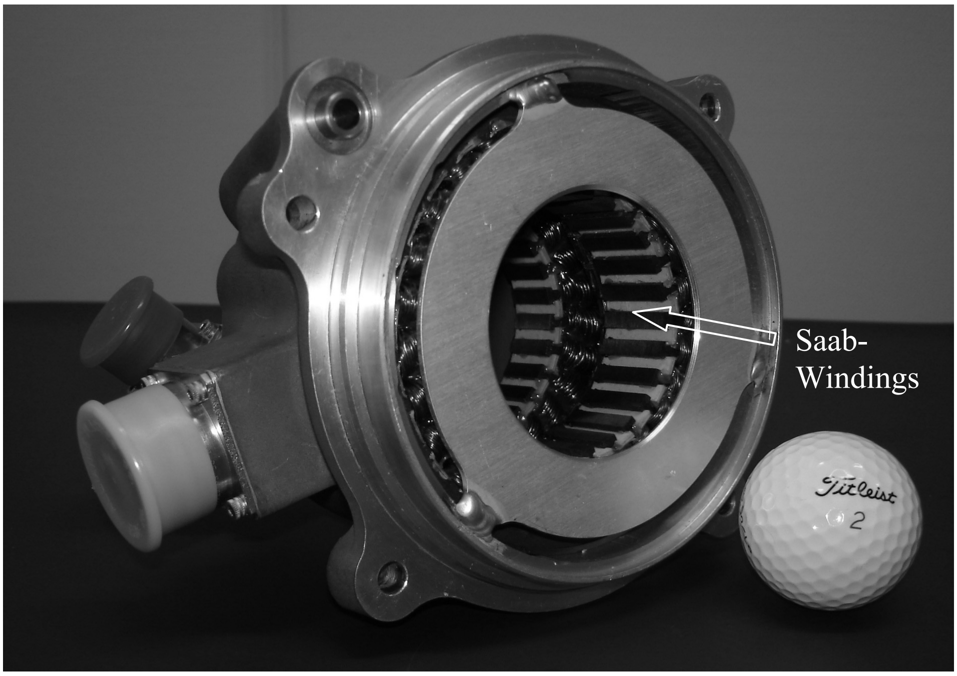

Fig. 53. The stator for the PM-generator used in JAS39 Gripen

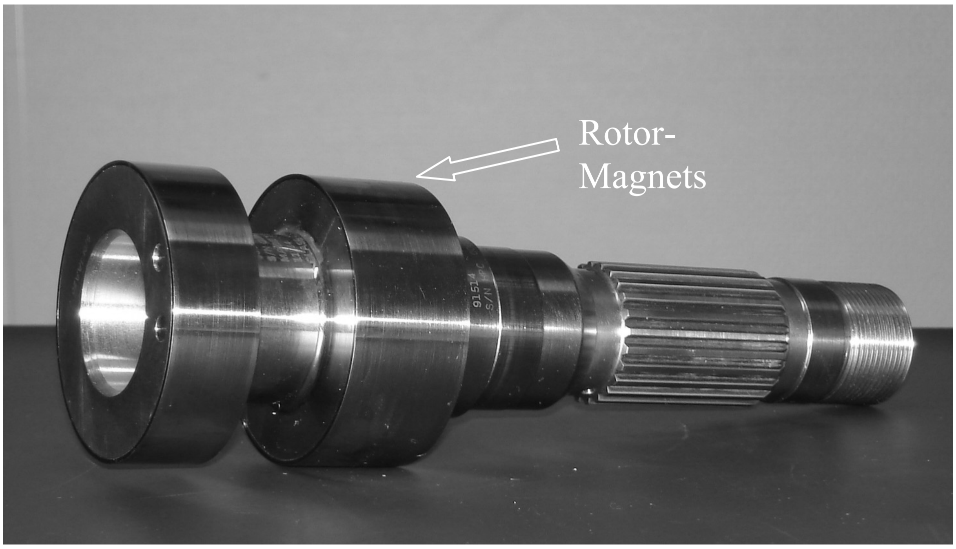

Fig. 54. The rotor for the PM-generator used in JAS39 Gripen

6.2 Future Power Systems

Without the restraints of the present standard and the limitation of equipment available from the product catalogs a better weight optimization could be achieved. Airframers are looking into the possibility of using double frequency and double voltage to gain weight. One question to be raised is whether a further increase of the frequency could be beneficial in aircraft electric power design.

Today's standard for an electric power supply system for an aircraft is in accordance with Mil-Std-704E, which specifies 115V 400 Hz, 28 VDC or 270 VDC. Airframers are currently looking into double frequency (or variable frequency up to 800Hz) and double voltage (3 x 230V AC) or 270 VDC and possibly +/- 270 VDC as the choice for future power supply.

By increasing the frequency, the equipment using magnetic circuits can achieve minimized weight of e.g. generators and transformers. System frequencies in the range of kilo Hertz for missiles, unmanned aerial vehicles (UAV) and other vehicles can be used when size and weight reduction is essential [10].

The alternative, with increased frequency, would give the advantage of reduced weight in the magnetic circuits, such as iron parts in generators, transformers and magnetic amplifiers.

The weight reduction is basically in direct proportion to the increase of frequency. However the full benefit might not be possible due to effects of skin depth and increased impedance in wiring as well as iron losses in the cores.

A Transformer Rectifier Unit (TRU) with the power rating of 3.5 kW, has a weight of 6.8 kg when operating at 400Hz. At 4 kHz the TRU could possibly have a weight less than 1.0 kg. This represents a considerable weight saving. The disadvantage with increased frequency is increased losses due to the skin depth effect and increased reactance in the wiring.

- By increasing the system voltage, the copper area can be reduced. Weight can be saved in the electric power distribution systems.

- By allowing variable frequency, the generator system can be simplified, and equipment for controlling the frequency can be excluded. E.g. the constant speed drive (CSD) can be diminished. The CSD represents about half of the weight of the generator. Typical aircraft generators are delivering 115/200 VAC with its frequency regulated to 400 Hz by the CSD. The CSD is commonly used in civil and military aircraft generators and is based on a hydrodynamic design. The leading supplier is Hamilton-Sundstrand, Rockford, IL.

An increased frequency opens new possibilities of using magnetic amplifiers and the equipment using magnetic circuits can be minimized regarding weight. By looking at the equation for designing transformers, $E=4.44 \cdot B \cdot A \cdot N \cdot f$, it can be understood that generators and transformers can get a lower weight in proportion to the increased frequency.

Beneficial for magamps is that electromagnetic emission (EME) is naturally low due to a soft switching characteristic between saturated and non-saturated state. The requested rectangular hysteresis loop for the magnetic material can be very god, but anything less than perfect implies soft switching and consequently low emissions. This reduces the requirements on the output filtering.

6.2.1 Skin Effect in Wiring

The disadvantage with an increased frequency is the skin depth effect allowing only the surface of a wire to be used to conduct the current [45].

The skin depth δ can be expressed:

$$\delta = \sqrt{1/\sigma\pi f\mu_0} \qquad (6.1)$$

For a copper wire with the conductivity $\sigma = 5.80 \cdot 10^7$ and a frequency of $f=$ 4000 Hz the skin deep will be approximately 1 mm.

This implies that the center part of the conductor, below 1 mm of the surface does not conduct current.

In JAS39 Gripen the wiring is 2 [mm²], with a radius of approximately a = 0.8 mm (an AWG 14 wire in accordance with the international wiring classification system). This wiring is used between the PMG-generator and the magnetic amplifier regulating the voltage supply of the electronic flight control system. The above implies that the skin effect is not a concern in the present Gripen design.

Example: At the radius a = 2 mm and a frequency of 4000 Hz. The skin factor can then in a simplified way then be expressed $k=A/A_{eff}$, where k>1.

The area $A = \pi(a^2) \approx 12$ [mm²]

A course approximation of the effective area then is $A_{eff} = \pi(a^2 - (a-\delta)^2) \approx$ 9 [mm²], i.e. effective area is then approximately reduced to 80 %. This corresponds to a wire with a radius of 1.73 mm (an AWG 8 wire) which can handle 65 Amp, at 115V, this gives 7.5 kW/phase and a total power of 22 kW in a three phase system. The use of double voltage 3 x 230 V would give a possibility to provide power levels of 45 kW. One way to handle the concern with skin effect, and to further increase the power output, is to use Litz wire.

The detailed expression of the skin factor R/R_0 is a more complex mathematical function involving Bessel functions as graphically illustrated in Fig. 55 [50].

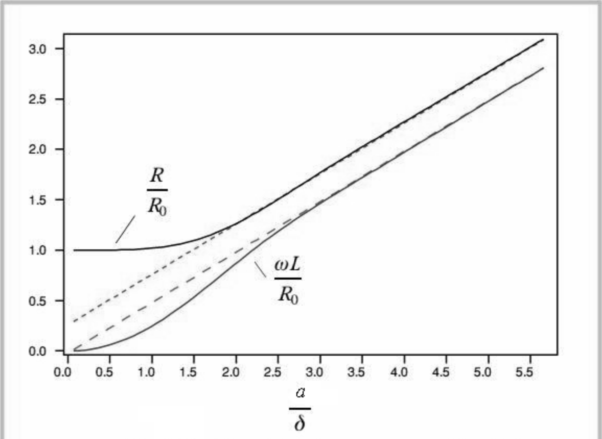

Figure 1 Wire impedance versus skin depth

Fig. 55. Shows the skin factor as $k=R/R_0$ as a function of a/δ

The two indicated methods of evaluating the skin factor give basically the same results when used in case 2-5 in section 5.5.2.

6.2.2 Increased Impedance in Wiring

A concern when approaching higher frequency could be the increased impedance in the wiring of the aircraft. An indication of the inductance L given by Eq. (4.2) for a double wire system and the reactance X (4.3) can be expressed as follows [47]:

$$L = \frac{\mu_0}{\pi}\frac{1}{4} + \frac{\mu_0}{\pi}\ln\frac{d}{a} \qquad [\mathrm{H/m}] \qquad (6.2)$$

$$X = 2\pi f L \qquad [\Omega/\mathrm{m}] \qquad (6.3)$$

Where *a* is the radius of the wire and *d* is the distance between the wires, center to center. It is assumed that the wires are twisted with a small margin for insulation. This can for example be *d/a*=3. The impedance increases at higher value for *d/a*. The presented impedances assume a temperature of 125 [°C].

For a 2 [mm²] (AWG 14) wire and a frequency of 4000Hz the impedance would be $X = 6.28 \cdot 4 \cdot L = 9.5$ [mΩ/m]. This should be compared with a resistance of app R =14 [mΩ/m] for 2 [mm²] (AWG 14). The impedance of the wire will be Z=R+jX. A total impedance of 16.8 [mΩ/m] is the resulting impedance in this example.

For a three phase system the reactance for each phase can be estimated by calculation of the values for a double wire system and recalculate the figures with the help of a correction factor, giving the reactance per phase. The correction factor used is a constant. In this example the correction factor 0.5 was used.

At 400 Hz the inductive contribution will change the impedance only a few percent (2.3 percent at 2 [mm²]) over the resistive contribution.

In Fig. 55 it can be noted that the relative impedance at 4000 Hz and 8000 Hz compared to the 400 Hz impedance increases with higher frequency and larger copper area (lower AWG).

In diagram Fig. 56 the absolute value of the wire impedance Z=R+jX is plotted as the total impedance for a wire installation and as a function of the wire area in [mm²].

With the given conditions, it can be noted that the impedance increases approximately by a factor 1.7 for 2 [mm²] (AWG14) when increasing the frequency from 400 Hz to 8000 Hz.

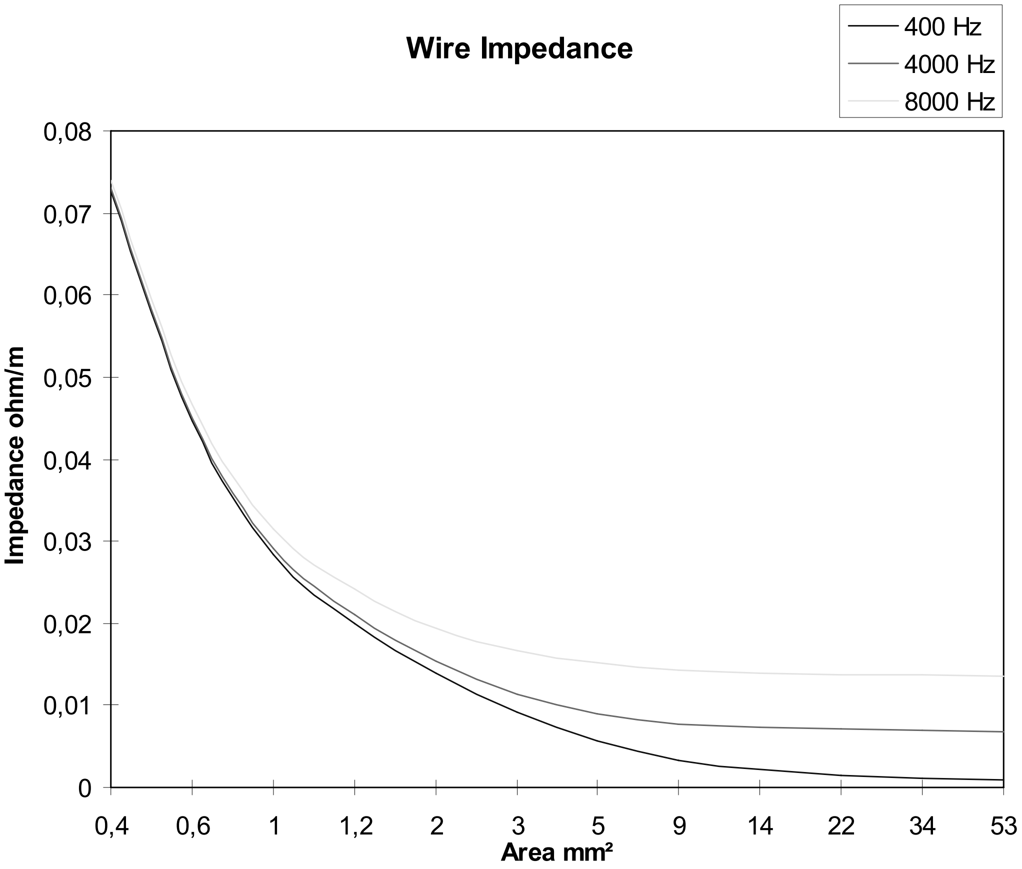

Fig. 56. Shows the absolute value of the one phase wire impedance, for a three phase system as a function of the conductor copper area for *d/a*=3

The increased impedance can not be compensated for by increasing the copper area, since the inductive contribution will increase even if the resistance is lower. At areas larger than this the proportion of the inductive contribution increases.

6.3 Feasible Concepts

A feasible concept comprises a generator supplying the system with a power frequency of e.g. 4000 Hz. A multi pole high-speed generator would offer improved power-density.

With technology of today the power conditioner e.g. a Transformer Rectifier Unit (TRU) working with 400Hz and a power rating of 3.5 kW, has a weight of 6.8 kg. At 4000 Hz the TRU could have a weight less than 1 kg. A considerable weight reduction could evidently be accomplished at higher frequencies.

A general concern in the design of electrical power systems is the power factor. One reason for the concern is the reactive power since this decreases the usable power. This is indicated by the fact that the generators are normally specified in kVA. We produce current and voltage that are not producing effective power, due to the inductive loads and inductive wiring.

The relative increase of inductive voltage loss can be acceptable at lower power levels, around 40 kVA that are suitable for a fighter or an Unmanned Aerial Vehicle (UAV). For a doubled three phase voltage (3 x 230V AC) the current peak would be 58 A, giving a voltage drop of approximately 0.5 V/m at 4000 Hz. AC-distribution with the length of 4 m, would still keep the voltage drop within the acceptable limit of 2 V.

In larger aircrafts such as airliners the reactive losses will increase due to increased length of wires that could be in the magnitude of 30 [m] or more. Normally large aircraft are equipped with four or five generators. The power rating of each generator then is as high as 250 kVA. At a doubled voltage the rated current will be as high as 362 A. This current will normally be split on two or three power wires, which offer the advantage of lower reactance (not analysed here).

The proposed concept with a high frequency generator and a power conditioner as shown in Fig. 57, is based on a high frequency distribution system and has the advantage of enabling the use of a Transformer Rectifier Unit (TRU). This can be an advantage since TRU:s are extremely reliable components. A TRU can have as low failure rate as less then ten failures (loss of function) [48] in a million flight hours.

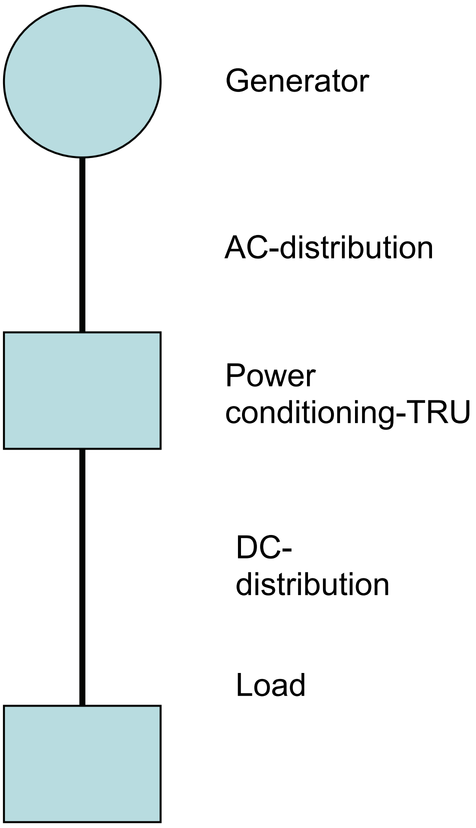

Fig. 57. Shows a simplified aircraft power supply system

The power conditioning unit can be designed with magamp technology having a regulation span of a few percent. A feasible design can be in accordance with Fig. 58 [46].

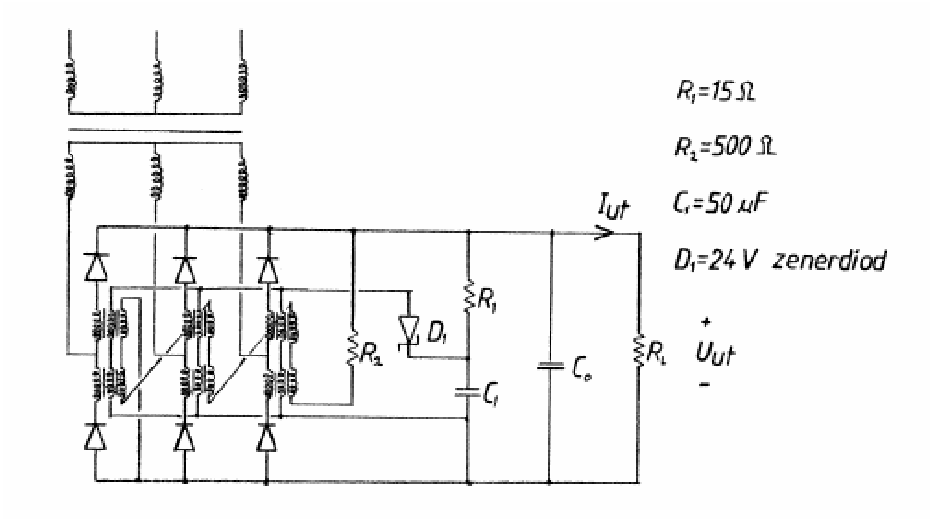

Fig. 58. Shows a TRU with controlled output voltage [46].

AC-net, using regulated AC-power for loads

Normally in an AC-net reactive compensation could be arranged in order to compensate for the reactive load. Such reactive power compensation can be performed with magnetic amplifier technology.

K. Nakumura proposes a Variable Inductor that is a magnetic amplifier controlling the current in an electric power grid [26]. The advantage claimed is high efficiency and that the unit is suitable for high power levels.

The presented unit was intended for a stationary power distribution system. The variable reactance produces 1.2 kVAr, reactive power at 10 Amp primary current. Only 20W iron losses are produced. A 1.2 kVAr unit rated 300 kVA at a frequency of 50 Hz weights 3.9 ton. In a power net application the windings are connected in delta and in parallel with capacitors. A 3D-simulation was performed to include the leakage losses.

Reactive effect compensation can be performed with technology similar to a magnetic amplifier. Equipment with a superconductive controllable reactor can be studied in T. Wass, Licentiate Thesis [27].

Reactive compensation for wiring could be performed with series capacitors in order to compensate for the reactive wiring. This can be in combination with reactive compensation.

DC-net, not using regulated AC-power

In a DC-net where no regulated AC current is used reactive voltage drop in the wiring can be accepted. If the generator is unregulated, the voltage might fluctuate due to variation of the input speed of the generator. These voltage variations will be transferred to the accompanying DC-distribution system. A magamp regulator could offer advantages to obtain a constant DC voltage of e.g. 270 VDC.

Regarding DC-systems there are problems to find appropriate circuit breakers, because the physical sizes of such breakers are considerable.

The increased impedance (reactance) due to a higher frequency in the wiring can not be compensated for, by increasing the wire area. In an aircraft installation the distance between phases and distance to structure can be reduced. The voltage can also be increased, which reduces the required size of the wires.

A system optimization should include the impact and effects that the electric power system could have on the other systems; this has been studied in ref [3].

The obtained results show that the magamp technology can offer interesting and competitive systems. The advantages with a magamp application must be evaluated from case to case and the outcome is depending on the specific set of parameters.

Chapter 7

Conclusions and Future Work

7.1 Conclusions

In this Licentiate thesis magnetic amplifiers and the operation of magnetic amplifiers are discussed. Different concepts are described and analysed by use of a detailed simulation model and proposed engineering tool.

Magnetic amplifiers are a not widely known today. Nevertheless the technology is of interest especially in high reliability applications. The high reliability and robustness also represent a significant value adding to the attraction of magnetic amplifiers in aircraft applications. The primary use today is as voltage regulators. New soft magnetic materials, such as amorphous magnetic alloys, have enabled the use of magnetic amplifier technology in the design of competitive electric power circuits.

The studied magnetic amplifiers indicated very high efficiency as well as low weight when operating at high frequencies. The chosen core material is very important for the final result when designing a magamp.

The methods for calculating the losses are based on different methods. By using algorithms provided by the vendor or hysteresis models core characteristics and losses is simulated for a proposed design.

By simulation during one or more full cycles of operation of the magamp its behavior can be studied. Electrical data as current and voltage can then be analyzed by studying the hysteresis loops. Based on the flux and magnetic field the iron losses can be analyzed.

The used algorithms and methods to evaluate the losses and specifically the iron losses work very well. The performed simulations indicate very god efficiency of the magamps as well as the feasibility to design them for high power-density.

The model is in this work used to simulate the behavior of a magnetic amplifier and to evaluate losses. The used model can be very useful since it is a dynamic model that can be used for any magnetic amplifier application regardless operating frequency. Furthermore this simulation model of hysteresis losses can be used for any magnetic circuit, as e.g. transformers.

The described system integration concepts indicate that the operating conditions for the magnetic amplifiers can offer advantages such as low weight low losses and high reliability.

7.2 Future Work

In further work the models will be verified by comparing the simulated results with tests. Calorimetric analysis is a feasible method to use.

The models need to be updated in accordance with test results.

The models should be extended for a variety of feasible materials of interest, in order to better be able to evaluate suitable alloy for specific applications.

The deviation from perfect squareness of the core magnetization curve is defined by B_r/B_s, see Fig 18. It must be considered during design but can according to the reference [28] be compensated for to some extent by the control circuitry. This will be further analyzed in future works.

Saturable reactors may be used as switches to discharge pulsed energy in high power microwave weapons [11]. This and other electric power applications of different magamp circuits are to be evaluated and further studied.

References

[1] L. Austrin, J.H. Krah and G. Engdahl: "A Modeling Approach of a Magnetic Amplifier". *Proc. of the International Conference of Magnetism*, Rome, Italy, 27th July-1st August, 2003.

[2] L. Austrin, and G. Engdahl: "Modeling of a Three-phase Magnetic Amplifier". *Proc. of the 24th Congress of the International Council of the Aeronatical Science*, Yokohama, Japan, 29th August-3rd September 2004.

[3] B. Johansson, L. Austrin, G. Engdahl, P. Krus: Tools and Methodology for Collaborative Systems Design Applied on More Electric Aircraft. *Proc. ICAS 2004, Yokohama*, Japan, 29th August-3rd September 2004.

[4] L. Austrin, J. Hansson: "New Electric Components for Aircraft", *Proc. Flygteknik 2004*, Oktober 18-19, 2004 Stockholm (In Swedish).

[5] P. Krus, B. Johansson, L. Austrin: "Concept Optimization of Aircraft Systems Using Scaling Models". *Proc. Recent Advances in Aerospace Actuation Systems and Components*, November 24-26, 2004 Toulouse, France.

[6] L. Austrin, D. Ribbenfjärd, G. Engdahl: "Simulation of a Magnetic Amplifier Circuit Including Hysteresis". *Digest for Intermag* . Nagoya , Japan, April 2005.

[7] L. Austrin, D. Ribbenfjärd, G. Engdahl: "Simulation of a Magnetic Amplifier Circuit Including Hysteresis". *IEEE transactions*.

[8] P Hallberg, L Austrin, P Krus: "Low Cost Demonsatrator as a Mean for Rapid Product Realization with an Electric Motorcycle Application". *Procedings of IDETC/CIE 2005*.

[9] M. Howse: "All Electric Aircraft" *IEE Power Engineer*, Volume 17 Issue: 4, Aug-Sept 2003 pp. 35-37.

[10] G. M. Attura: *Magnetic Amplifier Engineering*. McGraw-Hill New York 1959.

[11] A. G. Milnes: *Transductors and Magnetic Amplifiers*. McMillan&Co Ltd-New York, ST Martin's press 1957.

[12] E. R. Hnatek: *Design of Solid-State Power Supplies*. Van Nostrand Reinhold Company, New York, 1971.

[13] W. A. Geyger: *Magnetic Amplifier Circuits*. McGraw-Hill, New York, London, 1954.

[14] H. W. Katz: *Solid State Magnetic and Dielectric Devices*, John Wiley & Sons Inc 1959.

[15] B. V. Nilsson: *Ernst Fredrik Werner Alexandersson*. ISBN 91-972360-6-3

[16] A. Bergqvist: *Physica B Condensed Matter*, Elsevier, 233, p. 342, 1997.

[17] D.C. Jiles: “Modelling the Effects of Eddy Current Losses on Frequency Dependent Hysteresis in Electrically Conducting Media”. *IEEE transactions on magnetics vol 30*, no 6, nov 1994.

[18] R. Richter: *Elektrische Maschinen*. Band 1, Birkhauser Verlag, Basel 1951.

[19] Metglas product information, www.metglas.com

[20] B. Johansson, L. Austrin, G. Engdahl, P. Krus: “Tools and Methodology for Collaborative Systems Design Applied on More Electric Aircraft”. *Proc. ICAS 2004*.

[21] Alexander Grimeton, Veteranradions vänner.

[22] G. Bertotti: *Hysteresis in Magnetism*. Academic Press, Inc. 1998, ISBN:0-12-093270-9

[23] Dymola, www.dynasim.se

[24] S. Lemoine: *The Alexanderson High frequency Generator*. Tekniska meddelande Kungl. Telegrafstyrelsen Stockholm 1921(In Swedish).

[25] Lundahl Transformers, Norrtälje, Sweden

[26] K. Nakumura, et al: “Three Dimensional Reluctance Network Analysis Considering an Iron Loss Characteristic for an EIE-Core Variable Inductor”. Graduate School of Engineering Tohoku University. *Proc. ICAS 2004.*

[27] T. Wass: *Losses in high-temperature superconducting tapes in longitudinally applied magnetic fields*. Licentiate Thesis, Stockholm 2003.

[28] R.M. Tedder: ”Limitations of the Magamp Regulator and an Improved Magamp Choke Design Procedure”, *Proc. IEEE Applied Power Electronics Conference*, 1988 Record, pp. 109 - 117

[29] C. Jamerson: “Calculation of Magnetic Amplifier Post Regulator Voltage Control Loop Parameters”, *Proceedings of the Second International High Frequency Power Conversion Conference*, April, 1987, pp. 222-233.

[30] I. J. Lee, D. Y. Chen, Y. P. Wu, and C. Jamerson: “Modeling of Control Loop Behavior of Magamp Post Regulators”, *Proceedings of the Eighth Annual Power Electronics Seminar*, Virginia Polytechnic Institute and State University,” September, 1990, pp. 227-234.

[31] D.Y. Chen, J. Lee, and C. Jamerson: “A Simple Model Predicts Small-Signal Control Loop Behavior og Magamp Post

Regulator", *Proceedings of the Third International High Frequency Power Conversion Conference*, San Diego, Ca, May, 1988, pp 69-84

[32] H. Dean Venable: "Practical Techniques for Analyzing, Measuring, and Stabilizing Feedback Control Loops in Switching Regulators and Converters", *Proceedings of the Seventh National Solid-State Power Conversion Conference*, Powercon 7 Record, San Diego, CA, March, 1980, pp. I-12.1-I-12.17.

[33] C. Mullett: "New Amorphous Material Improve High-Frequency Saturable Reactor Output Regualtors", *Proc. Power Conversion and Intelligent Motion*, July, 1986, pp. 28-35.

[34] G. Engdahl, J. Krah: "Hysteresis model", *Journal of Magnetism and Magnetic Materials*, Vol. 242-245, Issue P2, April 2002, pp. 1210-1213.

[35] T.Higuchi: "A Statistical Model of Core Noise in Half-Wave Push-Pull Magnetic Amplifiers". *Proc. IEEE Transactions on Magnetics*, Dec 1970.

[36] R. Hiramatsu, et al: "A Magnetic Power Controller of Amorphous Cores for a 200 kHz Switching Regulator", *Proc. IEEE Transactions on Magnetics*. vol-18, no.6, Nov 1982.

[37] T. Koyashiki, S. Ohzora: "Control Characteristics in a Magnetic-Amplifier-Controlled DC-DC Converter". CH 2523-9/88/0000-0390, *Proc. IEEE*, 1988.

[38] T. Yamaguchi, et al: "Core Noise and an Anomalous Phenomenon in Amorphous Tape Wound Cores used for Sensitive Magnetic Amplifier", *Proc. IEEE Transactions on Magnetics*, vol. MAG-22, NO.5, Sept 1986.

[39] M. E. Eaton: "Adding flux paths to SPICEs analytical capability improves the ease and accuracy of simulating power circuits". *Proc. IEEE*, 1998.

[40] R. Hiramatsu: "Re-entrant characteristic of Magnetic Amplifier A New Analysis", *Proc. IEEE*, 1988.

[41] K. Murakami: "An Experimental Study of Flux Presetting-Resetting Characteristics of Magnetic Cores with Rectangular Hysteresis Loop", *Proc. IEEE Transactions on Magnetics*, 1965.

[42] K. Harada: "Applications of Magnetic Amplifiers to High-Frequency DC-to DC Converters". *Proceedings of the IEEE*, vol-76, no.4, April 1988.

[43] C. Jamerson: "Techniques for Reduction of Required Hearoom in High-Frequency Magamp Postregulators", *IEEE Transactions of Power Electronics*, vol-8, no.1, January 1993.

[44] S. Nakajima: “Loss Evaluation of Amorphous Saturable-Core”, *IEEE Transactions on Magnetics*, vol. MAG-23, no.5, Sept 1987.

[45] S. Ramo, J. R. Whinner, T. van Duzer: *Fields and Waves in Communication Electronics*. John Wiley & sons, New York, 1965, pp. 288-293.

[46] D. Eckerström: *JAS39 a Regulated Transformer Rectifier Unit*, Master Thesis, Chalmers, Gothenburg, 1993 (In Swedish)

[47] E. Hallén: *Electromagnetic Theory*. Chapman & Hall, London, 1965, pp. 250-252.

[48] EuroAtlas, Bremen, “TRU-product information”

[49] P. Westberg: ”Lundahl och den magnetiska förstärkaren”, *High Fidelity*, no 3, 1997, pp. 18-20. Audio Media A/S Kopenhagen, Denmark (In Swedish).

[50] Scots: Guide audio skineffect, pp.1. www.st-andrews.ac.uk

List of Symbols

Symbol	**Quantity**	**Unit**
A	Area	[m²]
A_{Cu}	Cross-section area of the conductor, copper	[m^2]
a	Radius of the wire	[m]
B	Magnetic flux density (Tesla [T] = [Vs/m²])	[T]
B_r	Residual magnetic flux density	[T]
B_s	Saturation magnetic flux density	[T]
$\hat{B}$	Amplitude of the mean flux density	[T]
D_m	Inner diameter	[m]
d	Distance between conductors	[m]
d	Ribbon thickness of core material	[m]
f	Frequency	[Hz]
G	Parameter of magnetic domains	[-]
H	Magnetic field	[A/m]
H_c	Coercivity force	[A/m]
h_{Fe}	Flux path length	[m]
I	Current	[A]
J	Current density	[A/m²]
$k_{windFactor}$	Winding factor	[-]
k	Skin factor	[-]
k_h	Empiric constant, hysteresis losses	[-]
L_{tot}	Total inductance	[H]
l	Length	[m]
m	Mass	[kg]
N	Number of turns	[-]
P	Power loss	[W]
P_{iron}	Power losses, iron	[W]
P_{CU}	Power losses, copper	[W]
p	Number of phases	[-]
R	Resistance	[ohm]
R	Reluctance	[A/Vs]
T	Temperature	[°C]
T	Cycle time	[s]
t	Time	[s]

U	Voltage	[V]
V	Volume	[m³]
W	Energy	[Ws]
w	Width of the core ribbon	[m]
X	Reactance	[Ω]
Z_e	Impedance, electrical	[Ω]
δ	Skin depth	[m]
η	Efficiency	[-]
Θ	MMF	[A]
μ_r	Relative permeability	[-]
μ_0	Permeability constant	[Vs/Am]
$\rho_{Res,Cu}$	Resistivity of copper	[Ωm]
$\rho_{density}$	Material density	$\left[\frac{\text{kg}}{\text{m}^3}\right]$
σ	Conductivity of the material	[1/ohmm]
Ø	Magnetic flux	[Wb] = [Vs]
Ω	Resistance, conduction	[Ω]

Appendix

H	1[Oe] = $10^3 / 4\pi$ [A/m]
B	Magnetic flux density Tesla [T] = [Vs/m^2]
	Gauss 1[G] = 10^{-4} [T]
μ_0	Permeability for vacuum =$4\pi \cdot 10^{-7}$ [Vs/Am]

Index

Alexanderson, 3, 6, 92
Alloys, 27
Amorphous, II, 93, 94
Anhysteretic, 45, 46
Annealing, 30, 31
ASEA, 8

Bertotti, 47, 49, 92

Calorimetric, 90
Coercivity, 25, 95
Coercivity force, 25, 95
Compliance, 35, 50, 60
Constant, II, 32, 33, 34, 46, 80, 82, 87, 95, 96
Current, 3, 9, 13, 14, 15, 17, 18, 19, 21, 23, 24, 30, 31, 33, 43, 55, 56, 57, 58, 59, 64, 66, 67, 68, 71, 73, 74, 80, 84, 86, 87, 89, 92, 95

Design, I, 1, 2, 8, 9, 10, 11, 13, 15, 22, 23, 24, 26, 27, 29, 37, 43, 66, 67, 68, 69, 73, 74, 75, 77, 79, 80, 81, 84, 85, 89, 90, 91, 92
Dymola, II, 10, 49, 92

Eddy current, I, 9, 11, 31, 33, 34, 47, 48, 49
Efficiency, 9, 27, 41, 55, 59, 66, 70, 73, 74, 86, 89, 90, 96
Energy, 32, 34, 90, 96
Equivalent, 43, 44, 48
Equivalent circuit, 44
Experimental, 50, 75, 93

Flux, 68, 73, 93, 95
Flux density, 9, 22, 25, 32, 33, 60, 61, 62, 66, 74, 95, 97
Frequency, I, 2, 3, 5, 6, 7, 8, 9, 11, 22, 32, 33, 34, 46, 60, 61, 64, 66, 68, 70, 71, 73, 74, 77, 79, 80, 81, 82, 83, 84, 86, 87, 90, 92, 93, 95

Generator, II, 92
Grimeton, 3, 4, 5, 6, 7, 92
Gripen, I, 1, 2, 24, 37, 38, 40, 77, 78, 81

Impedance, 7, 79, 82, 83, 87, 96
Inductance, 21, 43, 82, 95

Lamination, 96

Magnetic circuit, I, 3, 79, 80, 90
Magnetisation, 5, 45, 46
MEA, II, 1, 9
Methods, 2, 75, 89, 90

Permeability, 27, 30, 96, 97
Play operator, 45, 46
Power, I, II, 1, 2, 3, 6, 7, 8, 9, 10, 11, 13, 14, 15, 17, 19, 20, 22, 23, 24, 26, 31, 32, 33, 34, 38, 52, 53, 54, 55, 56, 57, 58, 59, 61, 66, 67, 69, 73, 74, 77, 79, 81, 84, 85, 86, 87, 89, 90, 91, 92, 93, 95
Pseudo particle, 45

Ramey, 8, 19, 20, 21, 22, 26, 69
Reluctance, 92, 95
Resistance, 7, 21, 64, 74, 82, 83, 95, 96
Resistive losses, 75

Short circuit, 7
Simulation, I, II, 9, 10, 12, 43, 49, 50, 51, 52, 55, 56, 57, 58, 59, 74, 75, 86, 89, 90, 91
Steinmetz, 3, 33

Temperature, 24, 55, 68, 82, 92

Voltage, 68, 73, 92, 96